The University of Maine
DigitalCommons@UMaine

Electronic Theses and Dissertations | Fogler Library

Summer 8-18-2023

Wave Attenuation Through Submerged Oyster Aquaculture Cages

Liam T. Hanley
University of Maine, liam.hanley@maine.edu

Follow this and additional works at: https://digitalcommons.library.umaine.edu/etd

 Part of the Hydraulic Engineering Commons, Oceanography Commons, and the Other Engineering Commons

Recommended Citation

Hanley, Liam T., "Wave Attenuation Through Submerged Oyster Aquaculture Cages" (2023). *Electronic Theses and Dissertations*. 3849.
https://digitalcommons.library.umaine.edu/etd/3849

This Open-Access Thesis is brought to you for free and open access by DigitalCommons@UMaine. It has been accepted for inclusion in Electronic Theses and Dissertations by an authorized administrator of DigitalCommons@UMaine. For more information, please contact um.library.technical.services@maine.edu.

WAVE ATTENUATION THROUGH SUBMERGED OYSTER AQUACULTURE CAGES

By

Liam Hanley, B.S. University of Connecticut, 2021

A THESIS

Submitted in Partial Fulfillment of the

Requirements for the Degree of

Master of Science

(in Civil Engineering)

The Graduate School

The University of Maine

August 2023

Advisory Committee:

Kimberly Huguenard, Associate Professor, Department of Civil and Environmental Engineering, Advisor

Lauren Ross, Associate Professor, Department of Civil and Environmental Engineering

Neil Fisher, Lab Manager and Instructor, Department of Civil and Environmental Engineering

WAVE ATTENUATION THROUGH SUBMERGED OYSTER AQUACULTURE CAGES

By Liam Hanley

Thesis Advisor: Dr. Kimberly Huguenard

An Abstract of the Thesis Presented
in Partial Fulfillment of the Requirements for the
Degree of Master of Science
(in Civil Engineering)
August 2023

Coastal erosion presents a growing issue to shorelines around the world and is especially harmful to Maine, a region where sea-level rise is higher than the global average. Green and hybrid coastal defense strategies are being implemented around the country to provide sustainable, habitat-friendly solutions to erosion control. Maine is a hotspot for commercial aquaculture, with an estimated $13.6 million economic impact. This study looks to bridge the gap between Maine aquaculture and the living shorelines initiative, by determining the wave attenuating properties of submerged oyster cages. The project will be able to inform local oyster farmers, resource planners, and engineers on the potential for submerged oyster farms to attenuate wave energy. This study aims to explore the idea of a working waterfront, where coastal resilience and sustainability are tied in with economic opportunity, all while encouraging the protection of habitats and water resources. This study utilizes field observations from several SOFAR Spotter Buoys deployed for 28 days that were positioned before and after a long line of bottom lying oyster cages to measure wave decay in a protected inlet of Casco Bay in the Gulf of Maine. These observations were combined with water level data from a HOBO water level logger to

assess the effect of tidal fluctuations. A computational fluid dynamic model complemented the field observations, which allowed for the characterization of the longitudinal wave decay along the farm. The wave attenuation mechanism was determined, as well as the wave-induced setup in mean water levels. The CFD model is a cut section of a long line of bottom-lying oysters, using DualSPHysics, a smooth particle hydrodynamic model. Wave decay of up to 80% for ~4 second waves was seen over 30 m of oyster cages, where less-steep waves and shorter waves were attenuated more. Added mass drag dominated wave attenuation compared to friction, supported by KC (Keulegan Carpenter Number) values <5. Given that waves generally attenuated by 30% over a narrow distance, this likely affected mean water levels through gradients in radiation stresses. Using a simple, cross-shore, wave- and depth-averaged momentum balance, set up in mean water levels reached up to 5 cm when including tidal currents. Barotropic gradients are known to drive currents, indicating that scaled-up versions of bottom oyster farms could have implications on coastal circulation in semi enclosed systems. Future research should explore optimization of bottom oyster farms to reduce a broader range of wave environments, while assessing the secondary effects of wave attenuation on ambient hydrodynamics.

ACKNOWLEDGEMENTS

"I know not all that may be coming, but be it what it will, I'll go to it laughing."

– Herman Melville, Moby Dick

I would like to thank my advisor, Dr. Kim Huguenard for this opportunity and guidance to study what I am passionate about with this project. Also, thank you to the U.S. Army Engineer Research and Development Center (ERDC) for their support and funding of my master's degree. Thank you as well to Dr. Lauren Ross and Dr. Neil Fisher for their general guidance in modeling and field techniques.

I'd like to thank my fellow coastal engineering graduate students, Matt, Sam, Lizzy, Nick, Nalika, Cristian for all the help and laughs. Although not directly involved with the project, these people were always around and willing to give advice on data processing.

And thank you to all of my people in Orono: Lily, Andres, Felipe, Jake, Eliza, JJ, Ashton, Casey, Aidan, Marsh Island Brewing Company, the basketball and soccer teams, and other graduate students in the department. Without you guys I would not have made it through this.

And finally, I'd like to thank my family, my parents, Chip and Kathy, for their unwavering support and interest in my academic life, and my brother, Kevin for his support and for giving our family art while I tackle science.

TABLE OF CONTENTS

LIST OF FIGURES

CHAPTER 1

INTRODUCTION

Wave attenuation over differing media has been a major subject of coastal engineering research for many years as a method of preventing coastal erosion. Here, an examination of the wave attenuation capabilities of bottom lying oyster aquaculture has been conducted. With proper design, aquaculture may be a sustainable coastal defense system. This study looks to further a research thrust at the University of Maine and look at the wave attenuation properties of Maine based aquaculture gear and systems. The first chapter introduces background information on coastal erosion, living shorelines, the working waterfront, previous studies in shellfish and aquaculture-based coastal engineering, as further chapters will expand upon these research thrusts with experimental techniques.

COASTAL EROSION

Coastal and estuarine shorelines are some of the most eroded habitats in the world due to their sensitivity to sea-level rise, increased wave energy from storms, and human industrial and recreational interactions, leading to loss of habitats as well as economic and societal losses (Scyphers et al., 2011). Resource managers and landowners around the world are increasingly worried about the present and future stability of shorelines (Manis et al., 2015).

Coastal erosion is prevalent in the sandy beaches of Maine, where 10 % of beaches are disappearing at a rate of two feet per year and 50% of beaches are disappearing between 1 and 2 feet per year (Slovinsky, Peter, Schmitt, 2011). While only 5% of Maine beaches are sandy

beaches that are considered to have very high shoreline change vulnerability, these beaches make up a significant part of tourism in the state and their loss is of great economic concern. Much of Maine's coastline is formed by "bluffs" or steep cliffs made of loose granular material that, depending on their stability, can be highly erosive. Loss of beach land and instability of bluffs can cause home and infrastructure damage due to undermining and landslides. The prevention of coastal erosion in Maine is an urgent issue (Slovinsky, Peter, Schmitt, 2011).

COASTAL PROTECTION APPROACHES AND LIVING BREAKWATERS

Traditional approaches to hardened shorelines, such as seawalls, breakwaters, and bulkheads have been used as coastal defenses to prevent damage caused by storms. However, these structures can worsen land subsidence due to poor soil drainage, prevent natural sediment accumulation by tides and waves, harm water quality, and destroy coastal habitats. Additionally, these hard engineering defenses require costly and continual maintenance, which is unsustainable given increasing flood risks (Zhu et al., 2020). Natural and nature-based infrastructure offer a more feasible solution to hardened shore protection, with added economic and ecological benefits, and the ability to adapt to sea level rise and climate change. In many commercial cases, nature-based solutions are being used alongside hard shoreline stabilization. Unlike conventional coastal protection techniques, nature-based coastal protection can mitigate storm damage and erosion while enhancing productive habitat, improving water quality, producing food, while adapting to rising sea levels. Wave attenuation devices can more effectively protect coastal ecosystems in areas with small tidal ranges and in exposed, high-energy areas, living shorelines require offshore structures such as breakwaters or sills to dampen incident wave energy to

promote healthy growth of the living organisms (Zhu et al., 2020). Living shorelines are a coastal stabilization strategy that involves the placement of native materials like plants, sand, and rock to reduce coastal erosion and encourage habitat growth. Specifically, this can be in the form of solid substrates with living plants, dune grass plantings, and artificial reefs and "living breakwaters" comprised of native species. Living shorelines protect from wave energy while maintaining a healthy ecosystem and natural littoral processes, resulting in a more sustainable coastal armoring alternative (Chauvin, 2018). A popular form of living shoreline design has been oyster reefs, or marsh sills filled with loose or bagged oyster shells (O'Donnell, 2017; Scyphers et al., 2011).The use of live oyster beds has been seen to impact waves by generating turbulence that disrupts the wave orbital velocities due to the roughness of the oyster colony, and combined with the land accumulation from planting, has been seen to slow and even reverse coastal erosion (Piazza et al., 2005; Scyphers et al., 2011). Generally, oyster reef living shorelines are planted with a hard substratum, such as pre-cast concrete or crushed limestone to promote growth from juvenile oysters. Breakwaters also come in the form of anchored bags of live oysters or oyster shells. The stacking of multiple bags has been thought to increase the vertical profile of oyster living shorelines (Morris, Bilkovic, et al., 2019). The hard geometry and roughness values of oyster beds and engineered oyster breakwaters attenuates waves both in field measurements and laboratory investigations. High structure/reef height to water depth ratio has been seen in experimental data to be well correlated to wave attenuation in laboratory experiments. Allen and Webb saw wave transmission coefficients reduce greatly with taller reef structures and higher wave heights for oyster shell bag breakwaters (Allen & Webb, 2011). In a field experiment, Chauvin et al (2018) observed wave transmission coefficients ($K_T = \frac{H_t}{H_i}$) from 0.11-0.62 for

varying breakwater heights and water depths for varying shaped planted oyster reef breakwaters from the Living Shoreline Demonstration Project in Southern Louisiana (Chauvin, 2018). Shellfish based coastal engineering has been seen to be a viable coastal defense system in field and laboratory experiments, however investigation into food production-based shellfish has not been studied for its wave damping capabilities. Aquaculture based shellfish structures, while similar in shape, are laid out in lines and could have greater attenuation properties.

MAINE AQUACULTURE AND OYSTER FARM SITE

In Maine, once-abundant oysters decreased drastically in population into the 20th century due to human impacts, however efforts from University of Maine researchers brought about the oyster farming industry in the state in the 1970s, focusing on the native species, *Crassostrea virginica* (Schmitt, 2017). Today, marine aquaculture in Maine continues to expand as a means of food production. In 2017, aquaculture in Maine had a $13.6 million-dollar economic impact, with oysters being the largest shellfish aquaculture market in the state (Schmitt, 2017).

It has been common practice since the 1970s for oyster farmers in Maine to layout their oyster farm in a floating array during warm months, using floating trays, or lantern nets suspended with floatation devices. This procedure is commonly used to grow oysters to market size quickly, but requires much more labor than bottom culture techniques (Main Sea Grant, 2013). Often in winter months, oyster farms are "overwintered" to prevent possible freezing on the surface in site conditions where bottom-lying oyster gear can be safely placed. Overwintered oysters are generally sunk to the bottom in wired cages filled with bags of oysters. These cages remain at depth during winter months and are generally undisturbed by farmers due to their

vulnerability from low respiration in cold water. Generally, bags of oysters that were secured in a floating array at the surface are combined into groups to be put in cages for the overwintering procedure (Main Sea Grant, 2013). This creates a high density of bagged oysters in cages. At Maine Ocean Farm in Freeport Maine, the study site for this project, 8 soft floating bags were placed in a 0.6-meter-tall winter cage (Figure 1). At the site of the oyster farm, the water level fluctuates from 1.5 to 5.5 meters, meaning that depending on the tidal stage, oyster gear takes up between 11% and 40% of the water column. This "shallow" water environment could allow waves to be affected by the oyster cage layout at the site.

Figure 1: *Example bottom lying oyster cage from Maine Ocean Farms from the field experiment. 8 mesh bags of oysters were stored at the bottom in a cage with large openings. Mesh bags were seen to be packed tightly with biomaterial. A floating long-line of the bags is seen in the background.*

"WORKING WATERFRONT"

The state of Maine defines working waterfront land as "a parcel, or portion of a parcel, of land abutting tidal waters or located in the intertidal zone (between the high and low water mark), that is used primarily (more than 50%) to 'provide access to or support the conduct of commercial fishing activities (Maine Revenue Service, 2020).' The idea of a working waterfront in Maine stems from the idea of the preservation of a marine based economy that faces many threats. Changing marine resources, increased gentrification, and pressures on fishing and aquaculture industries are all being intensified by the effects of climate change. With the coastline in Maine being such a driver for economic growth, the necessity to protect shores from coastal erosion remains at the utmost concern (Maine Coast Fishermen, 2022). Loss of land and critical ports in Maine would greatly restrict community access to the ocean and could prove detrimental to industries that keep the state alive. While not directly in the intertidal zone, oyster aquaculture wave attenuation could greatly affect erosion patterns of bluffs and beaches. If coastal erosion can be prevented with existing oyster aquaculture gear, it should be implemented where feasible.

Regulations due to the Natural Resources Protection Act of 1988 by the Maine Department of Environmental Protection virtually ban the construction of new "hard engineering" coastal structures in the state. With much of Maine's sand beach coastline owned by private entities, the state has struggled to apply public expenditures for coastal erosion protection measures. Property owners are also in a quandary as this strong regulatory approach to coastal preservation has not been fortified by a financial contribution from the government entity. The application of an

offshore, submerged, working-waterfront and nature-based system could provide a healthy solution to the regulatory problems the state of Maine faces when it comes to coastal protection (Emlein, 2021).

The potential of existing oyster aquaculture gear as a shoreline protection strategy was examined in a semi-sheltered cove of Casco Bay by determining if a longline of bottom lying oyster cages could attenuate wave energy. This field experiment was coupled with a numerical model that created a simplified, full-scale replica of the site which allowed for a deeper investigation into wave attenuation characteristics and processes. The research objectives of this thesis are to (1) determine the wave attenuation effectiveness of bottom lying oyster gear; (2) use a Smooth Particle Hydrodynamic numerical model to examine along-farm wave decay and to investigate the mechanism behind attenuation -form drag or added mass, and (3) investigate wave decay induced setup for implications to flow in a semi-enclosed basin.

CHAPTER 2

INTRODUCTION

Coastal and estuarine shorelines are sensitive to sea level rise and increased energy from storms (Scyphers et al., 2011). Living and nature-based coastal defense approaches, including shellfish-based breakwaters, reefs, and other structures, have become popular as a more environmentally friendly, sustainable, and sometimes economically sensible alternative to traditional “hard” shoreline defense (Allen & Webb, 2011; Morris, Bilkovic, et al., 2019; Scyphers et al., 2011; Zhu et al., 2020). Wave attenuation from shellfish and other rough body

natural and man-made features has long been studied, showing substantial wave decay in various forms and environments, including reefs, breakwaters, and engineered "castle" like structures (Allen & Webb, 2011; Chauvin, 2018; Piazza et al., 2005; Sigel, 2021). Aquaculture farms have also been studied more recently for their effectiveness as a coastal defense strategy.

Waves can be attenuated by as much as 92% by oyster shell bag breakwaters and oyster reef structures in emergent conditions, with a strong inverse relationship to an increasing dimensionless freeboard, which is the ratio of significant wave height to water depth, H_s/d. Wave attenuation via oyster shell bag breakwaters has shown some alignment to empirical design formulas (Allen & Webb, 2011, Allen & Webb, 2015, Van der Meer et al, 2005). Oyster castles (concrete structures housing oysters) in low energy environments (wave height < .5 m) can attenuate wave heights as much as 60% in near permanent emergence through porosity and overtopping (Chauvin, 2018). In highly macrotidal environments, wave energy flux is attenuated over planted oyster reefs as much as 80% through reflection, overtopping, breaking, and friction mechanisms, and have shown agreement with empirical design formulas (Sigel, 2021). Coral reefs, while not made of shellfish, function as frictional and bathymetric changes to the floor that can affect wave transformation as well. Coral reefs are very effective at attenuating wave energy, primarily through bathymetric change and secondarily through bottom friction, especially over the higher elevation reef crest- reducing wave heights as much as 97%, including longer period significant swell waves (Garzon et al., 2019). These reefs provide a coastal defense system through longer, longitudinal decay, and their resilience to storm damage should be further studied for impacts to wave attenuation. Longitudinal wave decay has been seen to cause setup in

mean water levels through changes in radiation stress gradients, with setups of up to 5 cm seen over fringing reefs, which can have impacts on currents and circulations in shallow, enclosed bays (Buckley et al., 2016). Other natural systems, such as kelp forests, can provide the same longitudinal decay of waves. Wave height decay of up to 80% has been measured over bottom secured kelp forests in shallow water depths (Morris, Graham, et al., 2019). Wave decay of bottom features is very limited by water depth, showing reduced effectiveness at higher water levels, due to the nature of wave orbitals occupancy of the water column, and studies have been limited to shorter waves (Allen and Webb 2011, Chauvin 2018, Sigel 2021). Sensitivity to water level is critical due to rising sea-levels and increased storm tides due to climate change.

Oyster based structures and other rough body coastal features have been studied somewhat extensively for wave attenuation, while aquaculture engineered approaches are a relatively novel insight. Aquaculture systems, due to their common layout in arrays or lines, can decay waves longitudinally like natural reefs and kelp forests. Floating kelp longline aquaculture has been seen to decay wave energy, through interaction with the flexible vegetation, up to 47% for shorter wave (T = 6s) in deeper water (~10 m) with less efficacy for longer, swell waves (Zhu et al., 2021). Decay was also seen to be linear in across-farm measurements for a similar structure (Zhu 2020). Likewise, floating mussel farms, a more physically rigid species secured to lines suspended in the water column, have been seen to reduce wave energy up to 20% in for 4 second waves in up to 11.5 m depth (Plew et al., 2005). Floating aquaculture wave decay is seen to be independent of water depth, due to their constant suspension in the water column, and will be unaffected by rising water levels and storm tides. One type of oyster aquaculture involves the

placement of cages full of bags of oysters at the bottom of the ocean for winter growth. Floating systems often need to be quite long to be effective (80% of the wavelength) (Giles et al., 1978). While floating systems struggle to attenuate longer waves (T > 10s) (Plew et al, 2005), bottom lying gear could have more success since they are not limited by the farm width to wavelength ratio as in floating structures. At shallower depths, oyster cages could take up a significant fraction of the water column as a bottom based structure, and flow through cages freely moving oyster bags could attenuate waves through mechanisms other than depth limited breaking seen in shell-bag breakwater studies (Allen and Webb 2011). Little work has been done in determining the wave attenuation mechanism of oyster aquaculture based coastal protection, which could have similar coastal defense benefits, while also adding to the burgeoning aquaculture industry.

The goal of this research is to study the wave attenuation performance of bottom-lying oyster cages and their potential effects on mean water levels. We quantify the wave attenuation properties of bottom lying oyster cages with field investigations of an overwintered oyster farm in Casco Bay in Maine. Then, a validated numerical model is utilized to investigate the wave attenuation mechanism, along farm decay, and applicability of an established empirical formula for submerged breakwaters. The empirical formula is used to inform wave decay induced changes in water levels in idealized scenarios. The chapter begins detailing the study area, followed by a discussion of the field observational campaign. Next, the numerical model used in this work will be introduced, followed by data processing analyses. The results section will show that waves are attenuated over an oyster long-line in the field observations. A discussion follows, which shows that wave attenuation is primarily through inertial drag and the resulting influence

on radiation stresses leads to a set up in water level that increases with tidal currents. Lastly, the discussion explores the generality of the findings by modeling the simulated wave decay with a tuned empirical formula for submerged breakwaters as a function of cage number. The main message emphasizes that oyster aquaculture may be an effective coastal defense strategy, though future research should cover a broader range of wave and water level conditions and assess the impacts of farm-imposed set up on coastal circulation.

METHODS

Study Area

Field investigations were conducted in the unnamed bay formed by the extended fingers of Wolfe's Neck and Flying Point near Middle and Maquoit Bay, located in the larger geographical coastal area of Casco Bay in Southern Maine (Figure 2). Casco Bay is a coastal system made up of multiple estuaries in the Southwestern Gulf of Maine. It is a hub for energy and boating industries as well as commercial fishing and recreational activities (Sinnett, 2012).The bay's morphology is defined by rugged bathymetry of channels, ledges and shoals, and an extensive layout of small islands created by glacial erosion and isostatic rebound. Casco Bay is fed primarily by the Royal and Presumpscot Rivers with mean annual discharge rate of 40 $\frac{m^3}{s}$, however sea water density distribution in this area is generally controlled by the larger Kennebec-Androscoggin River system, northeast and outside of Casco Bay, with a much larger annual mean river discharge of 300 $\frac{m^3}{s}$ (Sinnett, 2012). Winds in Casco Bay have large impacts on mixing with the discharge of the Kennebec River, as winter-winds from the northeast align

with the Kennebec channel allowing for more wind-driven exchange. Spring and fall winds generally show large magnitudes in the along-channel/winter (>10 m/s) direction (Sinnett, 2012). Generally, winds in the fall, winter and spring are from the north-northwest, with storm winds coming from the east and northeast. The average tidal range in Casco Bay is 2.75 m (Whiteman et al., 2016), and maximum tidal currents are around 0.36 m/s. Maquoit and Middle Bays have average water depths of less than 3 m in their shallower sections and experience wetting and drying throughout the tidal cycle (Spaulding, 2011).

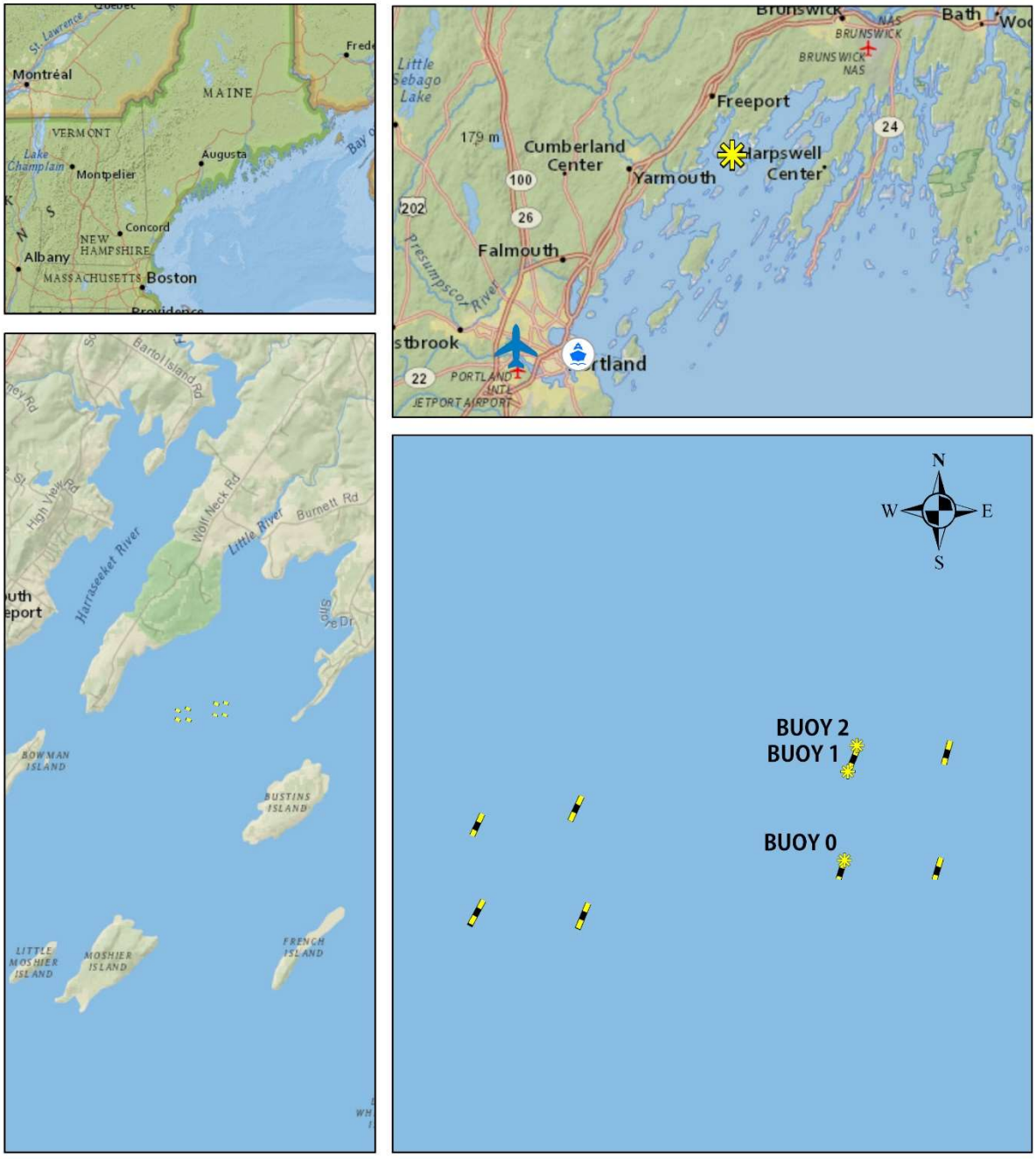

Legend

- Oyster Farm Long Line Location
- Portland Jetport
- NOAA Sta. 8418150
- SOFAR Spotter Location

Meters

0 110 220 440 660 880

Figure 2: *Study area map showing the northern east coast of the United States, the region of Casco Bay, and the nautical chart of Middle Bay with the positioning of SOFAR Spotter Buoy data collectors and the oyster farm lease. SOFAR Spotter Buoys are labeled 0, 1, and 2 as the offshore, and first and second long-line buoys, respectively. The location of the HOBO water level sensor is labeled. Other data streams of the Portland Jetport and Portland NOAA Station are labeled and in the legend. (Scale shown for bottom right panel).*

The oyster farm studied was owned and operated by Maine Ocean Farms- a Freeport, Maine based oyster farm. The oyster farm lease is in the central-southern part of the bay. The extents of the farm housed 80 overwintered cages laid in groups of 10 along a total of 8 long-lines that were 30 m in length (Figure 2). Cages were dropped in groups of 2 every 5 m, in a somewhat staggered array. Overwintered cages were 1.2 m long by 0.9 m wide, and stood 0.6 m tall, with each cage holding 8 soft, 1 m long floating bags of oysters.

Field Data Collection

Three SOFAR Spotter Wave Buoys were used to measure surface displacements in Middle Bay around Maine Ocean Farms. Buoys are labeled as buoy 0, 1, and 2 in Figure 2. Buoys 1 and 2 were placed on either side of the long line, 30 meters apart in the Northeast direction (Figure 2). Buoy 0 was placed further offshore 200 m from buoys 1 and 2 to capture more offshore wave conditions. The bathymetric change between the buoys 1 and 2 was negligible. Between buoy 0 and 1, the elevation change was 0.3 meters. SOFAR Buoys were tied off to the surface long line above the submerged cages with enough slack so they could float freely to collect wave data. The SOFAR buoys were set to record continuously at their sampling rate of 2.5 Hz. The SOFAR Spotter Buoys measured displacement in the X, Y, and Z direction, which was later used in directional wave processing. A HOBO Water Level Logger was also deployed directly adjacent to buoys 1 and 2 to capture tidal fluctuations in water level changes at the oyster farm long-line.

The HOBO sensor measured pressure every 5 min. Other data streams included wind data from Portland International Jetport, located 25 km from the study site, where wind magnitude and direction were sampled every 6 min. Barometric pressure data was taken from NOAA Station 8418150, located 21 km from the site, measured every 5 min.

Field Data Processing

Wave spectra were calculated from the x, y, and z displacements for 60-min segments. Displacement files were processed in segments with 30-minute overlap, where each spectrum was calculated with 3600 discrete Fourier transform points, segmented in 8 segments with a 50% overlap, for segments of 13.33 minutes. Roughly 900 waves were observed in each segment. In low wave environments (H < 0.35 m), elevated power at the lower frequencies appeared in the spectra due to GPS noise, which often resulted in a low frequency peak at periods of ~25 s. These instances were filtered out in preliminary data processing using cut off frequency of 0.199 Hz, where the tradeoff was losing any observations of swell during the measurement period.

Bulk wave statistics were calculated from each 60 min segment. Significant wave height, $H_{mo,}$ was calculated spectrally as the average of the highest 1/3 of wave heights during the collection period. In the frequency domain, H_{mo} was calculated use the following equation:

1

$$m_0 = \int_{w_{lower}}^{w_{upper}} S_{zz}\, dw$$

2

$$H_{m_0} = 4\sqrt{m_0}$$

where m_0 is the zeroth moment of the frequency spectrum, S_{zz} . w_{lower} was set at 0.199 as discussed previously and w_{upper} was 0.37. The peak period, T_P, was calculated as the inverse of the frequency at which the power is at maximum. Dominant wave direction was calculated as the direction of peak wave energy obtained from the Directional WAve Spectra Toolbox, (DIWASP) in MATLAB. Directional spectra were calculated for the frequency range ($0 < f < 0.5$), with directional bins of 10 degrees.

All directional analysis in this thesis, including wind and wave direction, is in meteorological convention- the direction in which the forcing is coming ***from***.

Wave Decay Analysis

To isolate waves that could be attenuated by the farm given farm depth and length, wave conditions were selected where the wavelength ($T > 5.0$ s) was smaller than the farm length and the wavelength ($T > 2.70$ s*)* was long enough that the waves could feel the cages at the bottom. For all water depths, waves with periods larger than 5 s had a wavelength larger than the length of the longline, indicating that the farm would not be acting on the full length of the wave. Generally, a bimodal spectrum represented wind sea with peak periods around 4 and 2 s as demonstrated in the example in Figure 10.

High and low frequency cutoffs were used to isolate the part of the wave spectrum that can be impacted by the farm. Wave statistics associated with waves that can experience farm decay

(periods ranging from 2.70 to 5.0s) were defined using the mean wave height, $\overline{H_F}$, and mean period, T_{pF}, where the subscript indicates waves experiencing farm decay and the overbar indicated the mean. These were calculated using an Upward Zero-Crossing Analysis for one-hour periods for periods of 2.70 to 5.0 s. Zero Crossing analysis is defined by measurements of period and wave height, using the relationship between water surface elevation and time intervals, where distance is marked between zero elevation and crests and troughs of waves to determine wave height, and distance between crossings is measured for period (Kamphuis, 2010). In order to understand along-farm decay with a finer resolution than before and after the farm, a numerical model validated with field observations must be utilized.

DualSPHysics Model Setup

A smooth particle hydrodynamic numerical model is used in this study in concert with field observations. DualSPHysics solves the SPH system of governing equations for weakly compressible flow is as follows:

3

$$\frac{d\rho_a}{dt} = \sum_b m_b (v_a - v_b) \nabla_a W_{ab}$$

4

$$\frac{dv_a}{dt} = -\sum_b m_b \left(\frac{(P_b + P_a)}{\rho_b * \rho_a} + \Pi_{ab} \right) \nabla_a W_{ab} + g$$

5

$$\frac{dr_a}{dt} = v_a$$

Where subscripts a and b represent interaction between two particles, t is time, r is position, v is velocity, P is pressure, ρ is density, m is mass, g is gravitational acceleration, and W_{ab} is the kernel function (Altomare et al., 2017). The system is closed by Tait's equation of state:

6

$$P = B\left[\left(\frac{\rho}{\rho_0}\right)^{\gamma} - 1\right]$$

Where $\gamma = 7$ as a polytropic constant, and $B = \frac{c_0^2 \rho_0}{\gamma}$, where ρ_0 is the reference density and c_0 is the numerical speed of sound. The DualSPHysics SPH model employs a dynamic boundary condition, using a set of particles that do not move with the forces exerted upon them. A piston wave maker is made up of boundary particles. The wave piston pushes the water particles to create waves (Altomare et al., 2017). To accurately model wave propagation in DualSPHysics, a density diffusion term, noted as "Fourtakas Full" is applied to reduce density fluctuations in the fluid domain. This dynamic density term is applied to these current models in this paper.

Bottom friction in DualSPHysics is generated by a viscosity factor for all boundaries, the "ViscoBoundFactor". The factor for viscosity in the numerical simulations is set to 1, in order to limit wave dissipation through viscosity interaction with the boundary or bottom. The ViscoBoundFactor is defined as:

$$ViscoBoundFactor = \frac{\alpha_{FB}}{\alpha_{FF}}$$

Where, α_{FB} is the interaction between fluid and boundary particles and α_{FF} is the interaction between fluid particles (Gormley & MacLeod, 2021). Using this factor, some numerical dissipation, was still seen (3-9% wave height decay), when cases were run with no oyster gear present, and this should be considered as a limitation.

The DualSPHysics model for this experiment was designed to be a simplified replica of the domain of the long line of oyster cages in a two-dimensional numerical flume. The flume was 60 m long with a piston wavemaker at one end and a sloped beach at an arbitrary angle of 14 degrees at the other (Figure 3). The piston and beach were designed with enough height to allow for water depth to fluctuate from 1.5 to 5.5 meters. This would cover the environmental conditions seen at the site to allow for model validation.

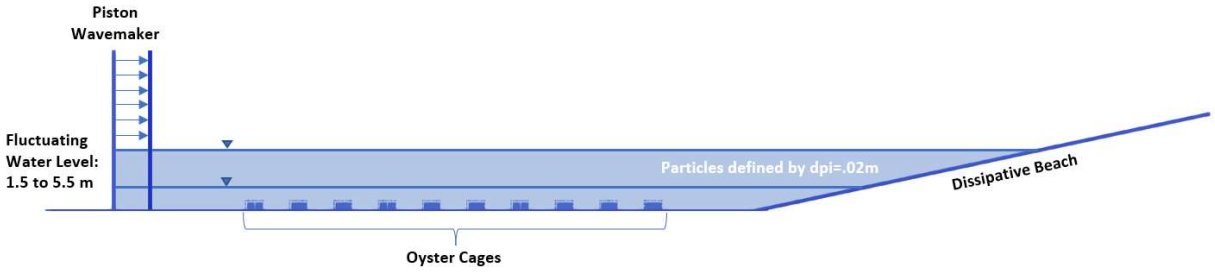

Figure 3: *Numerical flume designed in DualSPHysics. The piston wavemaker and dissipative beach are designed to accommodate 1.5 to 5.5 m of water depth while reducing reflection. The cages cover a 30-m span on the floor of the numerical flume. Water particles and boundaries are defined by an interparticle distance of 0.02 m.*

In the numerical flume, oyster cages were modeled as a grid of squares to allow for flow of water with equal total dimensions to field cages. Numerical porosity was not defined for the

cages as it is not developed for this model. Inside the grid of squares, 8 blocks were modeled as floating oyster bags. The floating oyster bags were given a relative weight of 0.9 to allow for some buoyancy. An example cage is shown in Figure 4a and 4b.

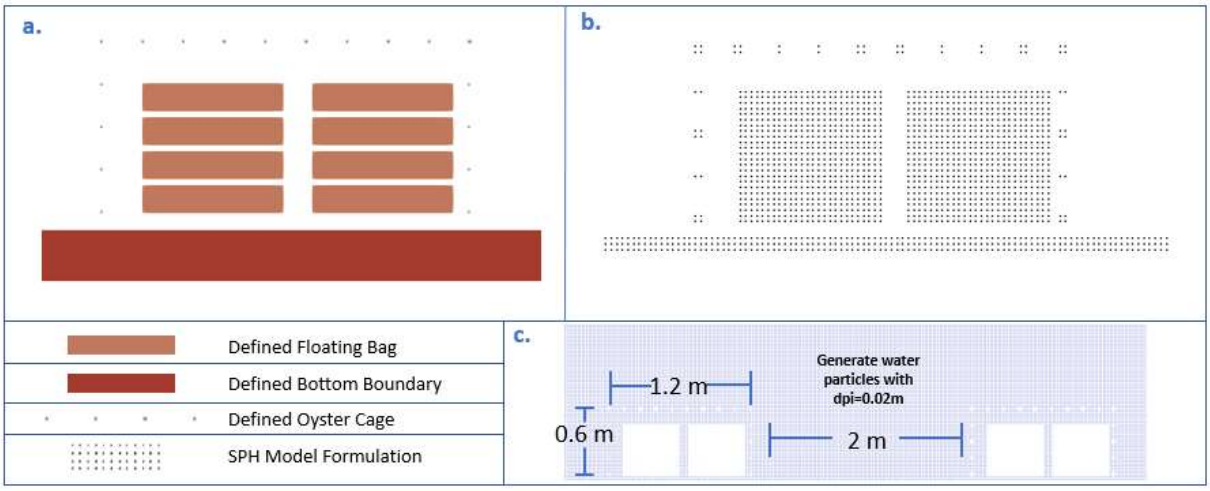

Figure 4: *a. Input defined geometry for floating oyster bag, oyster cage, and bottom boundary. The oyster cage was defined as small blocks to allow proper water flow into the cage for interaction with floating elements. b. Generated particles in numerical flume for defined geometry using an interparticle distance of 0.02 m. Oyster bags were generated in the model as 2 large floating blocks. c. Cages and floating bags in generated water particles for a depth of 1.5 m. 10 cages were spaced at 2 m.*

The long line of oyster cages was modeled in two dimensions as an evenly spaced line of 10 cages along 30 m, which differed slightly from the staggered layout seen on the site. This layout was chosen for simplicity, as the staggered layout was not possible in the 2-D simulation and could potentially cause some discrepancy between field and model results.

Model Parameters

The model parameters were chosen based on recommendations from model developers for wave propagation in DualSPHysics. All simulations were run with an interparticle distance, dp,

of 0.02 meters. With cases ranging between 2 m and 5.5 m in water depth, between 230,000 and 790,000 particles were generated in the numerical flume. The smoothing length h_{sph} was defined by the equation $h_{sph} = c_h\sqrt{3dp^2}$, where c_h is the smoothing length coefficient. c_h was tuned to 1.8 to allow for better results in wave propagation. The viscosity in the model was formulated using laminar viscous stresses and sub-particle scale turbulence (SPS). Wave generation in the model was forced with a JONSWAP spectrum. A significant wave height was calculated from the wave decay portion of the spectrum to force DualSPHysics with a JONSWAP to simulate the same wave cases seen in the field. These conditions were forced in DualSPHysics using the irregular wave piston wavemaker feature with a tuned up JONSWAP enhancement peak factor, γ, of 12. This γ value is larger than typically used (~3.3) but was found to fit well with the wave decay spectrum from field measurements (Figure 5) and a zeroth moment validation was conducted for wave generation synchronization (Figure 6). A dt value, or time-out value of 0.1 seconds was used, and this value was taken as the sampling frequency of the SPH model measurements, 10 Hz.

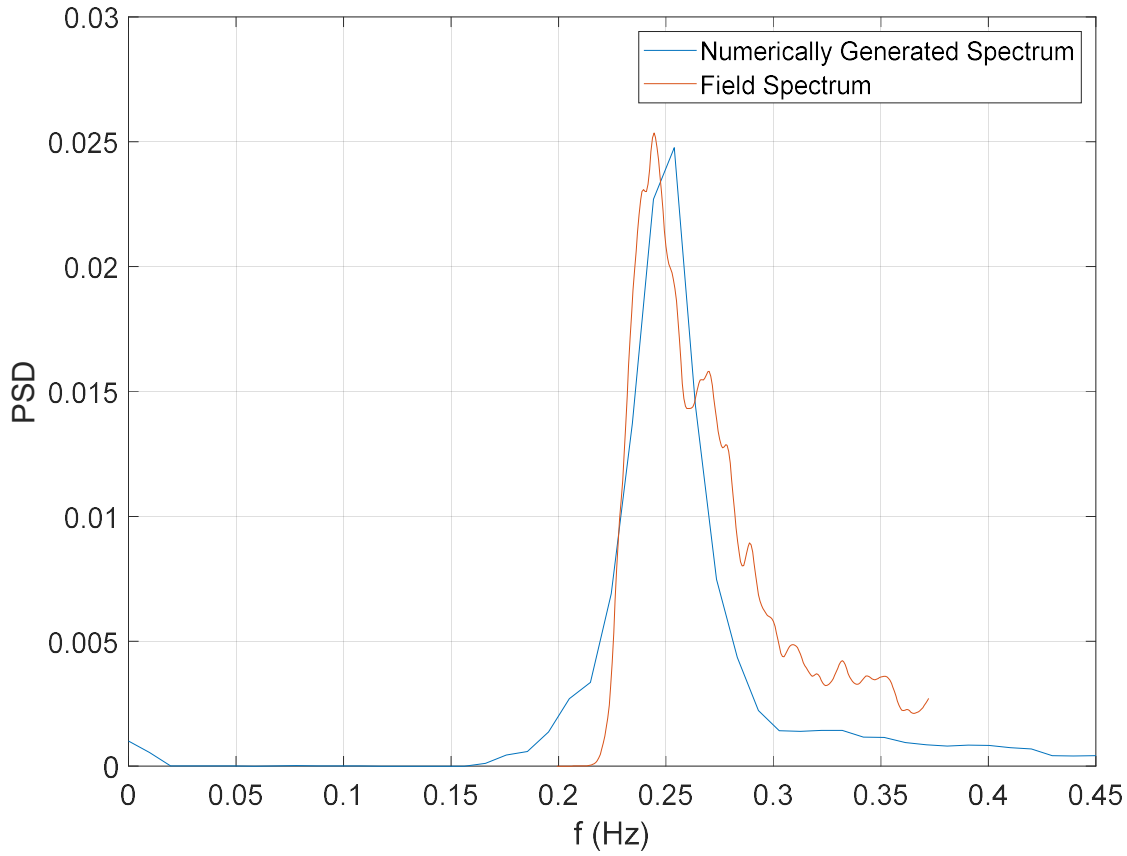

Figure 5: *Example comparison of numerically generated (blue) and field observed (orange) wave spectra from model validation.*

Water elevation was measured at 10 locations across the flume, spaced every 4 feet. The first elevation measurement measured the incident wave field, and the fourth measured the transmitted wave field. The two intermediate measurements were taken to analyze along-farm decay.

The DualSPHysics numerical model was validated by simulating the portion of the wave spectrum analyzed in the field conditions. Model validation focused on field occurrences that featured moderate wave heights (greater than 13.5 cm) and northerly wind directions ($300^{\circ} <$ dir

$< 45^{\circ}$). All cases had a run-time of $10 * T_{P_i}$ to allow for development of wave spectra. The conditions tested in the model and their results are displayed in Table 1.

Test ID	Depth (m)	Tested H_{S_i} (m)	Tested T_{P_i} (m)	K_{T_F}	K_{T_N}	R_{K_T}
1	1.55	0.16	4.10	0.71	0.18	0.35
2	1.96	0.16	4.09	0.52	0.41	0.82
3	1.98	0.20	4.07	0.94	0.45	0.11
4	2.07	0.16	3.87	0.94	0.44	0.11
5	2.32	0.17	4.02	0.92	0.58	0.18
6	2.34	0.20	4.06	0.62	0.57	0.87
7	2.45	0.18	4.16	0.54	0.61	1.16
8	2.98	0.17	4.16	0.63	0.64	1.01
9	3.46	0.19	4.01	0.59	0.64	1.13
10	3.60	0.16	4.03	0.94	0.57	0.13
11	3.94	0.18	4.11	0.70	0.65	0.87
12	4.25	0.19	4.06	0.76	0.76	0.97
13	4.40	0.18	4.15	0.48	0.77	2.29
14	4.81	0.15	4.04	0.77	0.84	1.47
15	5.34	0.15	4.09	0.92	0.93	1.19
16	2.96	0.14	4.07	0.83	0.63	0.45
17	2.13	0.16	4.11	0.80	0.47	0.37
18	3.36	0.13	4.20	0.76	0.64	0.66
19	4.73	0.14	4.04	0.74	0.84	1.61
20	5.24	0.15	4.15	0.50	0.79	2.36
21	2.20	0.14	4.08	0.75	0.52	0.52
22	2.62	0.14	4.06	0.88	0.57	0.28
23	2.49	0.14	4.10	0.68	0.56	0.74
24	4.15	0.13	4.20	0.96	0.66	0.13
25	3.22	0.14	4.16	0.65	0.60	0.86
26	4.31	0.14	4.02	0.63	0.82	2.00
27	4.41	0.13	4.10	0.62	0.76	1.60
28	2.66	0.15	4.09	0.84	0.56	0.36
29	1.98	0.14	4.07	0.86	0.36	0.21
30	4.02	0.13	4.02	0.67	0.68	1.02

Table 1*: Numerical test cases run for validation and investigation of along-farm decay, and parametrization of wave attenuation. 30 DualSPHysics cases were run on NVIDIA A100 GPUs.*

To ensure that the model was forced with the same incident conditions as the field, a wave forcing validation was conducted by comparing the zeroth moment, m_o, of the JONSWAP piston spectrum in SPH with farm decay portion of the spectrum from observations. The field and numerical m_o compared well with a linear fit and normalized RMSE of 0.1505 (Figure 17). Wave

transmission, K_T, was also compared between the model and simulation. Overall, the model is often over or under predicted K_T for several simulations and this is likely due external forcings (such as wind, currents, 3D effects) in the field observations that were not included in the simulations (Figure 16). While the model featured a single line of cages in a purely wave environment, the field observations consisted of nearby longlines, waves that propagated oblique to the longlines, and featured tidal currents, which likely contributing to discrepancies in some of the comparisons. However, there were a few instances where the model compared well with the simulations, which were used for further analysis.

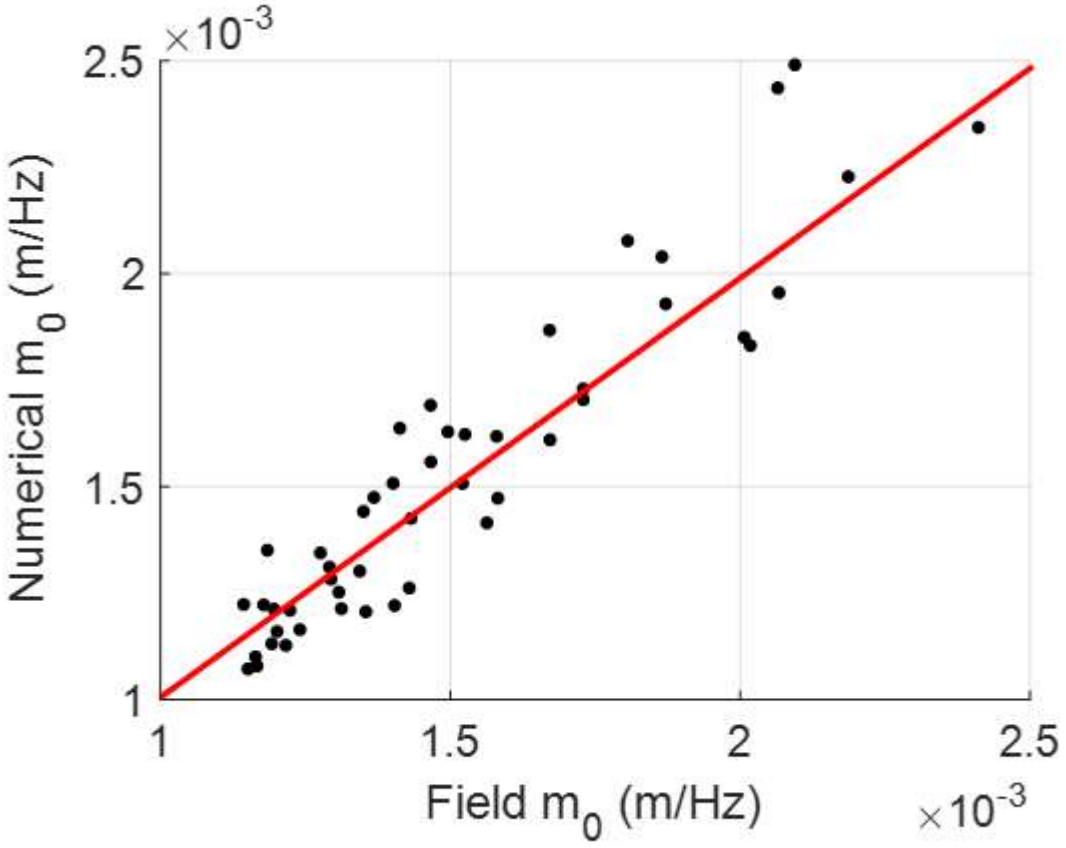

Figure 6: *Zeroth moment, m_o, comparison between observed field wave spectra and numerically generated wave spectra using the piston wavemaker in SPH.*

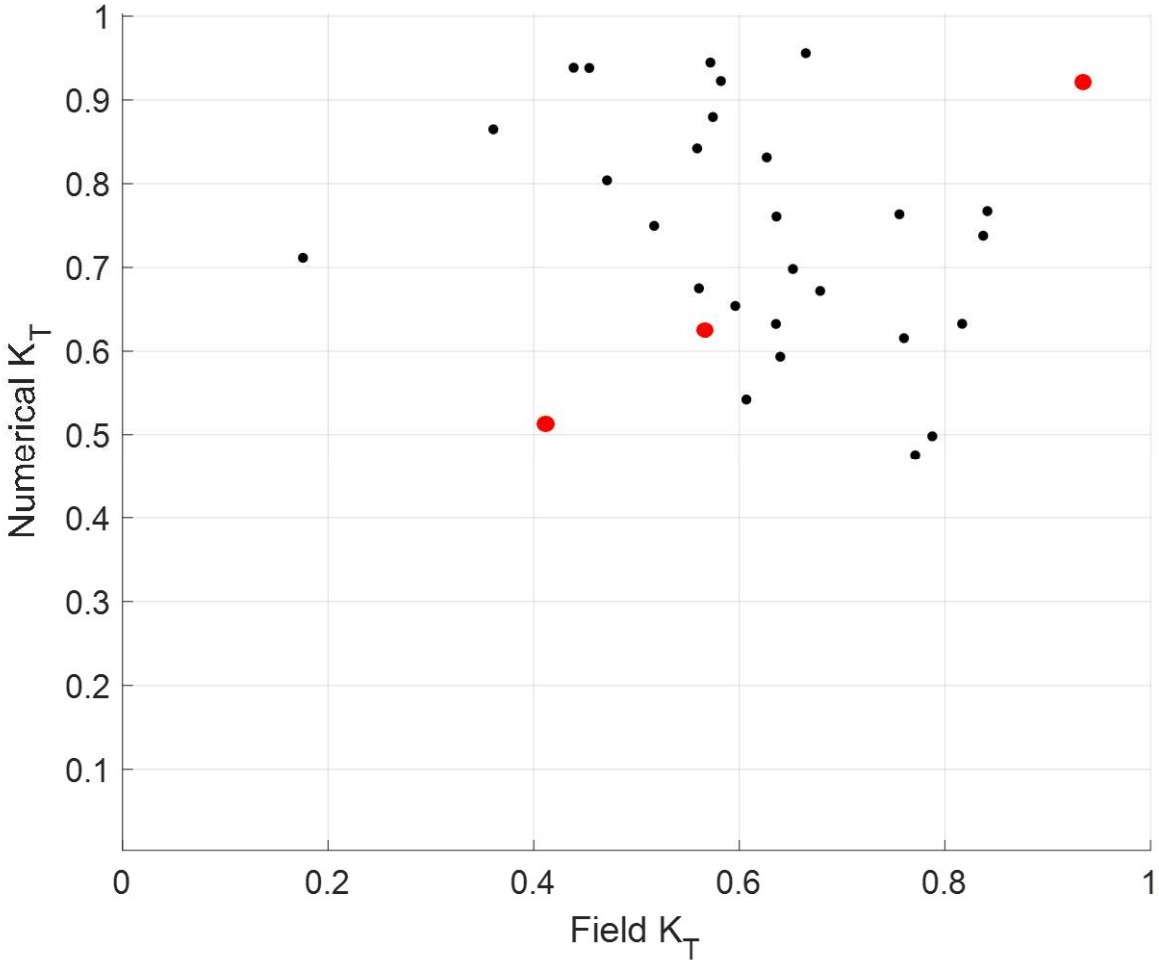

Figure 7: *Field and numerical K_T values comparison. Red dots indicate cases used in further analysis.*

Wave attenuation differences between the field and numerical simulations were compared using a ratio of the decay in the field to the decay in the numerical flume, R_{K_T}, where:

7

$$R_{K_T} = \frac{1 - K_{T_{FIELD}}}{1 - K_{T_{NUMERICAL}}}$$

Values of R_{K_T} over 1 indicate that the model underpredicted wave decay or attenuation in the field, and values less than 1 indicate that the model overpredicted decay in the field. It's clear that at lower water depths, the model overpredicted attenuation and at higher water depths the model underpredicted attenuation (Figure 8). In shallower simulations, over prediction may have occurred due to numerical diffusion of waves in the numerical flume, caused by low resolution simulation effects. Additionally, some complexities in field decay measurements could have underpredicted attenuation in the field, causing these discrepancies.

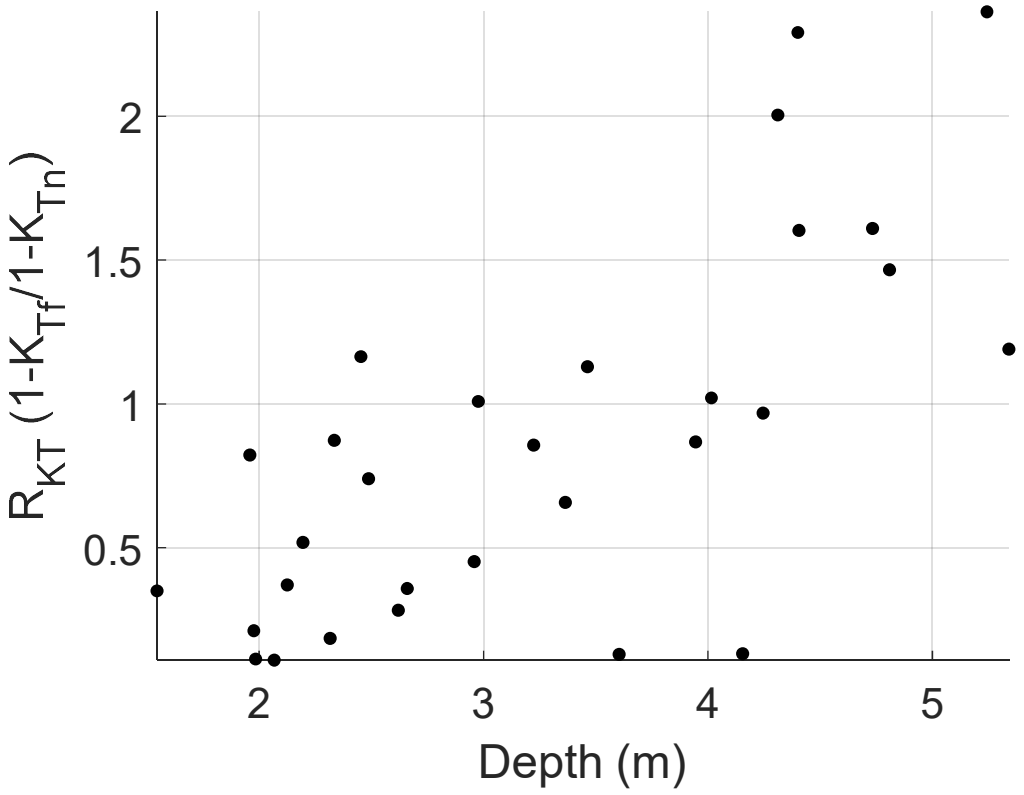

Figure 8: *Wave decay ratio, R_{TK}, as a function of water depth.*

RESULTS

Observations were collected during spring from April 6 to May 2, 2022. Wind speeds during this time varied from 0 to 12 m/s, with average wind speeds of 5.8 m/s (Figure 9a). Winds were primarily Northerly (offshore), as indicated by directions < 100˚ or > 250˚ (Figure 9b). Middle Bay is located in the interior of Casco Bay, therefore, the significant wave heights and peak periods were relatively small, ranging 0.1 m < H_s < 0.45 m and 1s < T_p < 4s, respectively (Figure 9c). Four storms occurred on April 8th, April 16th, April 22nd, and April 28th, as indicated

by drops in barometric pressure (Figure 9c) and wind speeds that reached 12 m/s. During these times, H_s increased while T_p decreased. Wave direction is much more impacted by winds during storms due to high wind speeds and the fetch of the bay, this resulted in smaller period waves than typical during the sampling period. Tides were predominantly semidiurnal with typical tidal ranges of 1.74 m during neap tides and 3.9 m during spring tides.

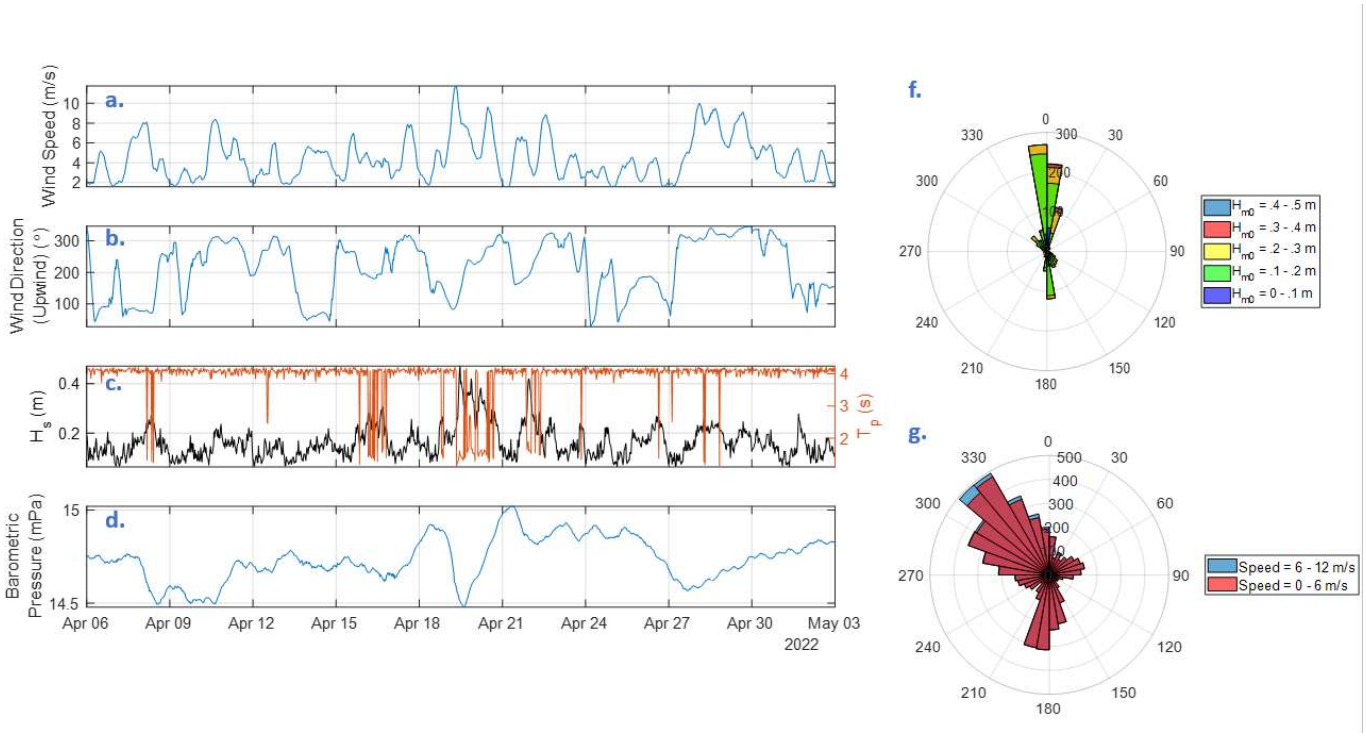

Figure 9: *a. Wind speed taken from Portland International Jetport. b. Wind upwind direction data taken from Portland International Jetport. C. Significant wave height is taken from the incident wave buoy, showing peak period and significant wave height across the data collection period. e. Wave magnitude and direction rose from SOFAR Spotter Wave Data. f. Wind magnitude and direction rose.*

The direction of the waves that can be influenced by the cages were predominantly from the North, propagating offshore (Figure 9f), which coincided with offshore northeasterly winds

(Figure 9g) and is typical of Casco Bay winds during summer and early spring months (Whiteman et al., 2016). Considering this, incident wave spectra were calculated at buoy 2 and transmitted waves were considered at buoy 1. Wave spectra was often bimodal, featuring two peaks, 0.25 Hz and 0.70 Hz, signifying wind sea and chop (Figure 10). Generally, more power was stored at the higher frequency peak (i.e., chop) than the lower frequency peak. However, waves in the higher frequency portion of the spectrum ($f > 0.5$ Hz) were deep water waves and could not feel the wave cages. Therefore, the portion of the spectrum of interest to understand how the oyster cages affect wave attenuation is $f < 0.37$ Hz.

When the wave decay region of transmitted and incident spectra is isolated (Figure 10), the energy between the two can be compared. The peak energy of deepwater waves ($f > 0.6$ Hz) is similar before and after the farm, which is consistent with the idea that these waves are not feeling the cages (Figure 10). However, an obvious reduction in energy after the wave propagates across the farm is observed at $f < 0.6$ Hz. Over the farm decay frequencies, the average wave heights, $\overline{H_F}$, varies from 0.05 m to 0.3 m, where smaller $\overline{H_F}$ corresponded to longer peak farm decay periods, T_{pF} = ~3.7 s, and larger $\overline{H_F}$ were linked to smaller T_{pF} = 3.1 s (Figure 11). The peak direction of the farm decay was similar to the peak direction of the full spectrum – from the north (Figure 11b). The wave direction of farm decay was mostly aligned with the orientation of the long line of cages, with the dominant direction being slightly more northerly than the long line orientation. Due to the orientation of the other long lines on the site, waves propagating in higher degree directions, closer to easterly, would have passed over additional longlines compared to waves from the Northwest, where no other longlines were present.

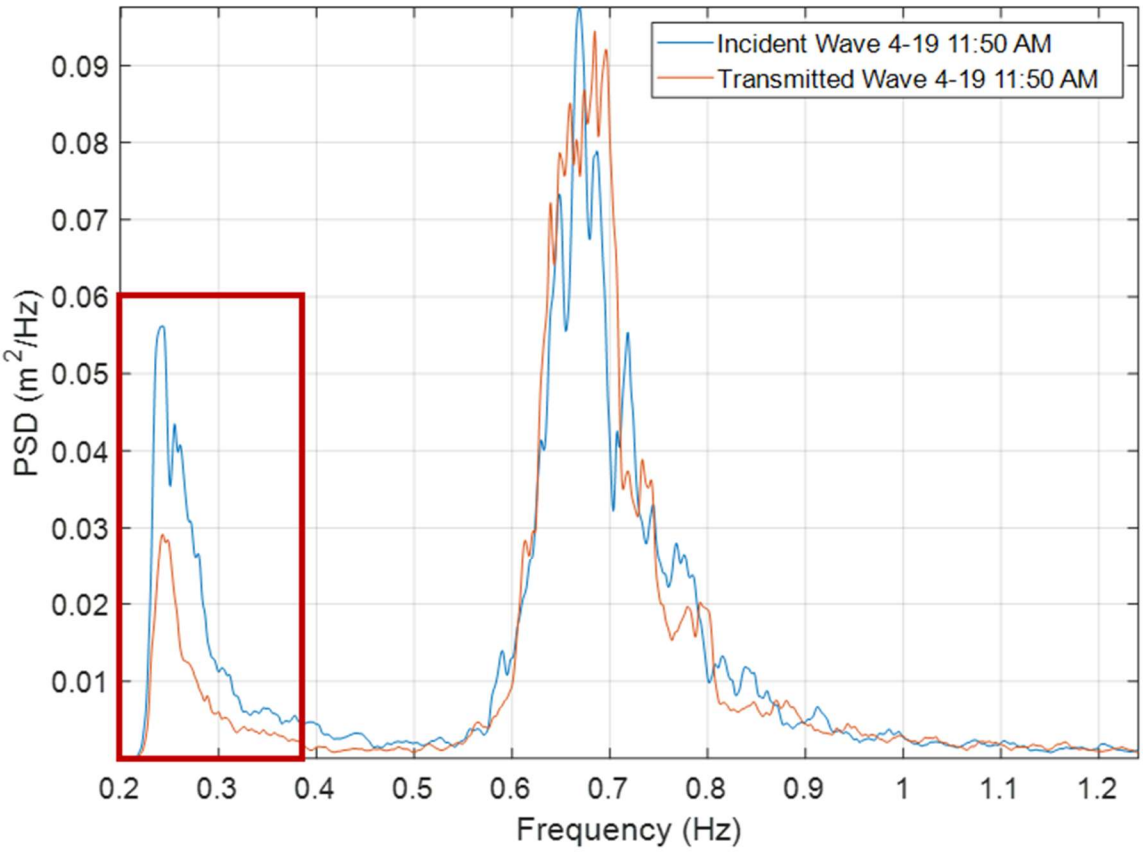

Figure 10: *Example full wave spectra for the incident and transmitted wave related to the long line of oyster cages. Typical bimodal spectra were observed with peak frequencies of around .70 Hz and .25 Hz, or 1.25 and 4.0 second waves.*

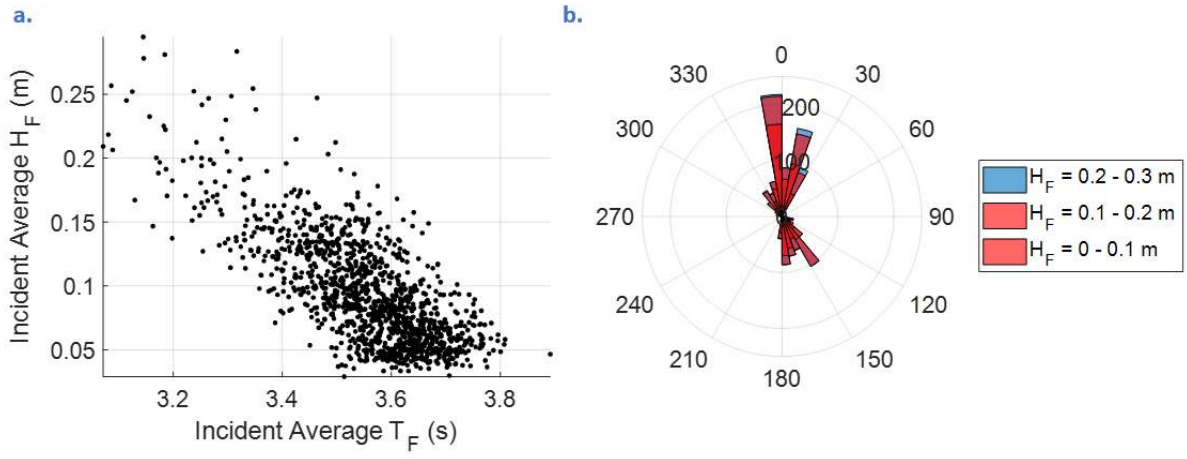

Figure 11: a. *Average wave parameters for the incident, influenced, wave field. Average wave heights and periods for the frequency domain were calculated using a Zero-Crossing analysis. Average wave heights studied ranged from 0.03 to 0.29 meters, and average periods ranged from 3.1 to 3.9 seconds. b. Influenced wave direction rose. Waves in this frequency domain propagated from the Northeast, out of the study area bay.*

The wavelength, L_F, associated with the peak farm decay frequency ranged from 11 m to 20 m, constituting a transitional wave regime with water depth to wavelength ratios, d/L_F, ranging from 0.11 to 0.33. Wave steepness, S, represents the ratio of the average wave height, $\overline{H_F}$, to L_F, and can be an indicator of wave breaking and shoaling in shallow water. S varied from 0.002 to 0.014, indicating that depth-limited wave breaking was not occurring.

To examine wave attenuation across the farm, a bulk transmission coefficient was calculated for each hour segment of data. A bulk transmission coefficient was calculated with

$$K_T = \frac{\int_{f_{lower}}^{f_{upper}} S_{zz_{transmitted}}\, df}{\int_{f_{lower}}^{f_{upper}} S_{zz_{incident}}\, df}$$

K_T quantifies the fraction of energy transmitted along the long line, where $S_{zz_{tranmsitted}}$ is the transmitted wave spectra for the segment, and $S_{zz_{tranmsitted}}$ is the incident wave spectra for the segment. Larger (smaller) K_T values indicate more (less) energy is transmitted, therefore less (more) wave attenuation. K_T values for the sampling period were bin averaged in steepness bins of 0.0025 width and wave direction bins of 10 degrees. Steepness binned K_T ranged from 0.68 to ~0.96, representing 32% to 4% wave attenuation, and generally increased with wave steepness, which implied that less steep waves resulted in greater wave attenuation across the longline (Figure 12a).

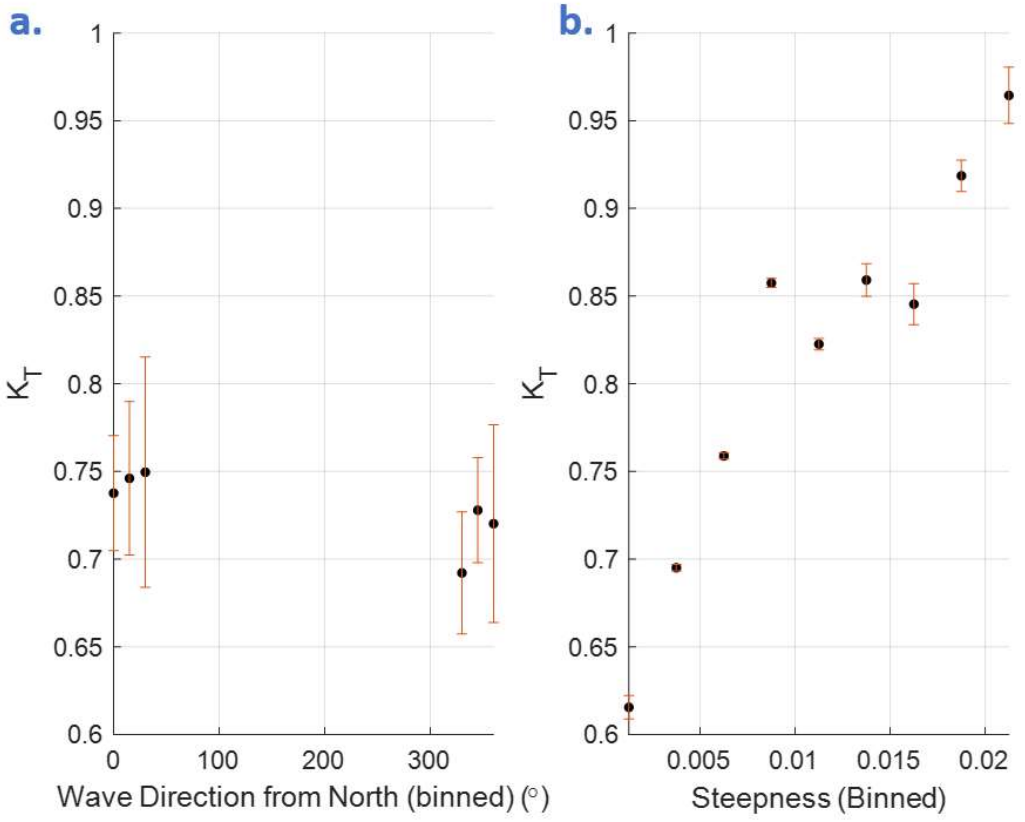

Figure 12: *Transmission coefficient, K_T, as a function of a. wave direction and b. wave steepness. Red bars represent 95% confidence intervals.*

When K_T was compared with wave direction over farm decay frequencies, θ_F, K_T generally decreased when wave direction was more northwesterly than northeasterly (Figure 12b). Comparing the farm orientation with wave direction (Figure 13), as θ_F is aligned with the along farm orientation (0-30°), K_T is smallest, indicating greatest wave attenuation. As θ_F moves into the northwesterly quadrant, the wave attenuation decreased, likely due to the orientation of the longlines having a reduced effect as waves approach more westward. K_T in the field

investigation did not show a trend with dimensionless freeboard, as it did in Allen and Webb (2011).

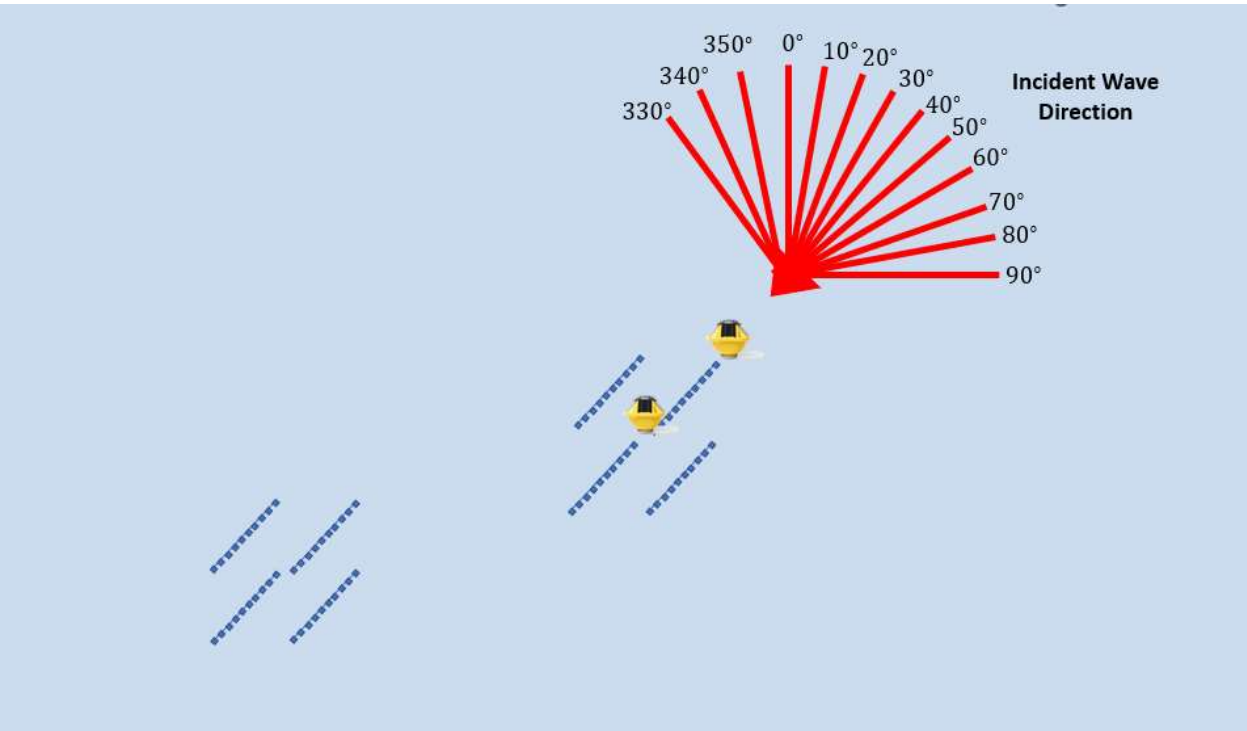

Figure 13: *Conceptual schematic depicting wave direction relative to the Maine Ocean Farms lease. Red square indicates the farm lease. Yellow symbols are wave buoys, the red arrows denote angles the waves are propagating from and blue squares are lines of submerged oyster cages.*

To examine how wave transmission varied by wavelength, the spectral energy was binned by frequency segments of 0.0063 Hz for the incident and transmitted wave fields. By integrating the spectral energy for each frequency bin, a transmission coefficient as a function of frequency, $K_{T(f)}$, could be derived by taking the ratio of the transmitted and incident integrated spectral energy. The wave energy by frequency bin was calculated using the following equation:

9

$$Segmented\ Power\ Variance\ (SPV\ (f)) = \int_{w_1}^{w_2} S_{zz}\, dw$$

Where w_2 and w_1 are the upper and lower bound of each frequency bin. A frequency dependent wave transmission coefficient, $K_{T_{(f)}}$ was calculated by the following equation:

10

$$K_{T_{(f)}} = \frac{SPV(f)_{transmitted}}{SPV(f)_{incident}}$$

$K_{T_{(f)}}$ were then bin averaged over the 25 frequency bins for the entire sampling period. $K_{T_{(f)}}$ decayed from 1 at f = 0.2 Hz to 0.63 at f = 0.35 Hz, indicating that wave attenuation was greater for shorter, higher frequency waves (Figure 14). While understanding of bulk decay in the field is important, an investigation into along-farm decay can provide more insight into the effect of wave reduction on mean water levels and currents.

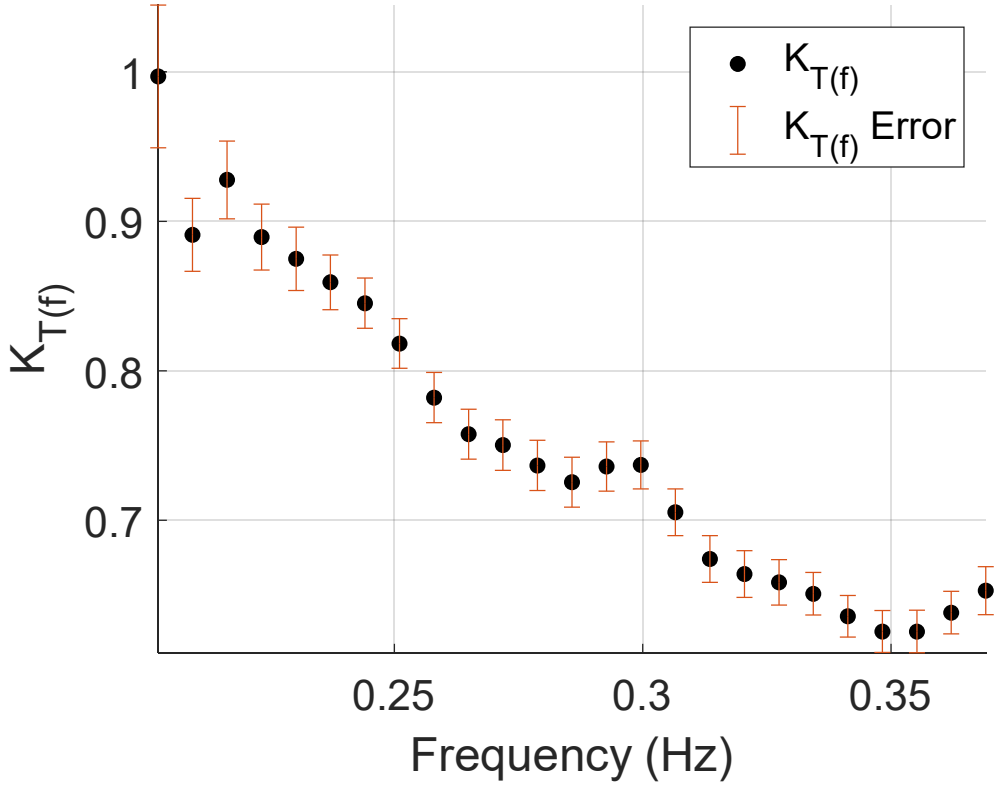

Figure 14: *Wave attenuation as a function of frequency, $K_{T(f)}$. Blue circles are the mean over the frequency bins and the red bars are 95% confidence intervals.*

Along Farm Decay

Due to the common orientation of aquaculture systems as arrays or lines, it is very important to examine "along farm" decay of waves along the longline so that longitudinal effects of coastal oyster farms can be parametrized and decay from larger farms can be predicted. Along farm decay was measured with 10 water level measurements across the longline in the numerical flume at 3 m spacing. Due to the similarity in all cases in wave height and wave period, four water depth cases were examined for zeroth moment decay (K_T) across the numerical flume, corresponding to high and low and one intermediary tidal water level seen in the data collection

period. K_T across the flume was seen to follow a downward trend with small fluctuations at higher water levels, most likely due to resonance (standing waves) over the long-line (Figure 15). These oscillations are similar to those seen in wave decay over a submerged canopy and can be attributed to the phase difference of reflected waves in the numerical basin (Chen et al., 2019; Zhu et al., 2021).

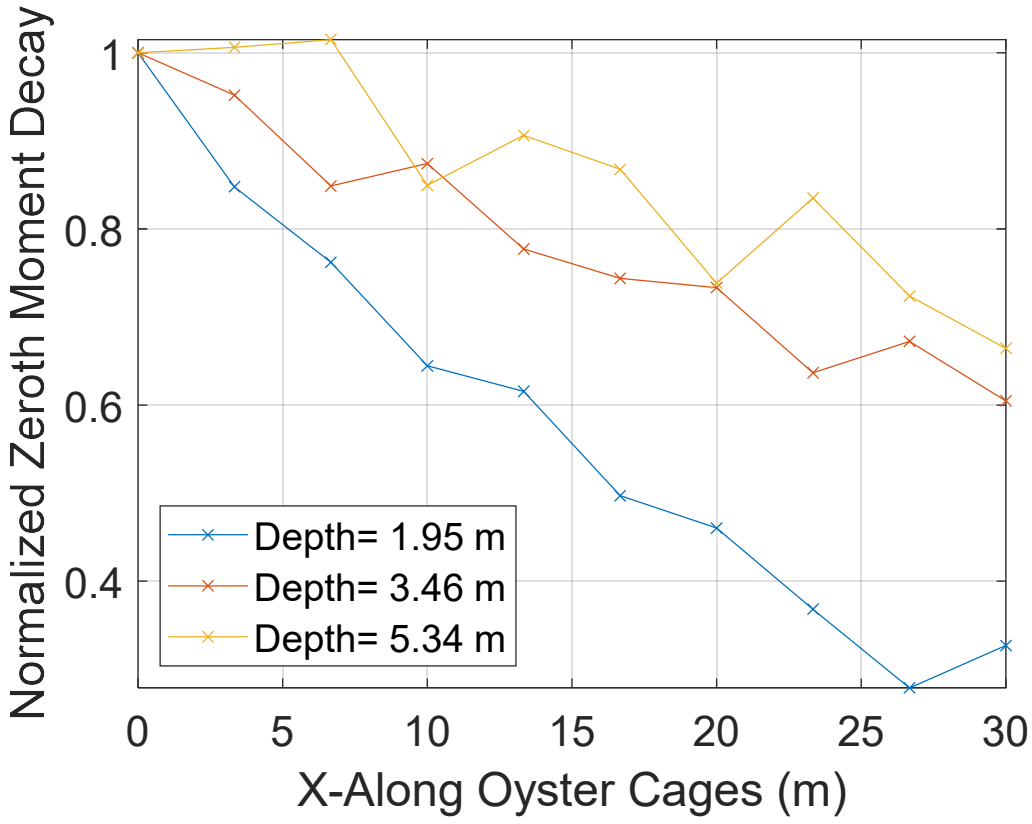

Figure 15: *Normalized zeroth moment decay along 30 m SPH flume.*

DISCUSSION

In the field investigation, wave spectral attenuation of up to 18% was observed in 4 s waves and 45% in 3 s waves over a 30-meter-long line of oyster cages (Figure 14). Wave transmission

coefficients showed the wave decay becoming more extreme as water depth decreases (Figure 16)- a finding consistent with oyster shell bag breakwaters in Allen and Webb (2011). Overall wave decay was higher over the line of cages compared to a single oyster bag breakwater for the same water depth and structure crest height scenarios. Decay was found to be mostly linear along the line length, alike to longitudinal decay seen over kelp farms (Zhu 2020). While water depths of 0.40 meters (deepest from Allen and Webb, 2011) were not observed in the field observations and no emergent cages were studied (Chauvin, 2018), wave attenuation was still seen to increase with lower water depths. The lowest water depth case studied (depth of 1.92 meters) yielded the most significant wave height decay over the longline (~45%). The findings of Allen and Webb (2011) focused on monochromatic wave transmission over a single oyster shell bag breakwater structure, while the present study investigated a line of less attenuative structures in an irregular and directional wave setting. The geometry of the oyster cages in general differed from that of previous studies, which could have impacted the wave attenuation mechanism. In Allen and Webb (2011) breakwaters were often sloped and occupied nearly the entire water column, therefore, while not discussed explicitly, waves were most likely attenuated by mechanisms of depth-limited breaking ($\frac{H}{D} < 0.8$) . In this study, the entirety of the outer structure was porous, so any depth-limited breaking/attenuation, commonly seen in Allen and Webb (2011), would have been lesser over oyster cages due to the porosity and deeper depths. Additionally, bags inside the cage were not fixed, allowing for floating bags to move from interaction with a passing wave. This could have created a transfer of momentum from the wave energy to the bags, inciting movement of the bags. This type of attenuation has been seen in novel floating breakwater design, where waves pass through floating balls in a cage, and attenuation is attributed to

absorption of wave energy in the balls (Ji et al., 2015). Further, the cages differed from the shell bag breakwaters in that the density of oysters in the structure was much smaller than in Allen and Webb's experiment, where the structures were made entirely of oyster bags with little voids (Allen and Webb, 2011). To understand if wave attenuation was dominated by frictional drag versus added mass from the structure, the Keulegan–Carpenter number was investigated.

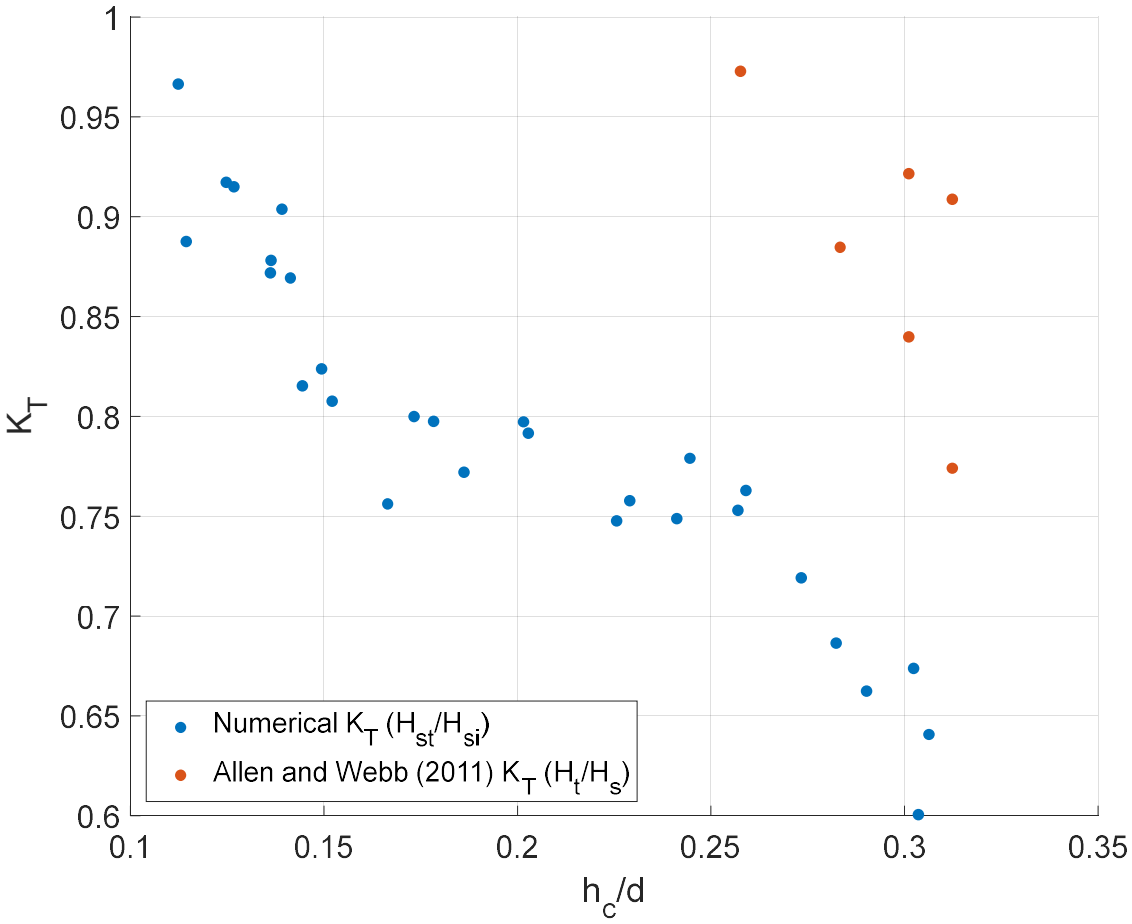

Figure 16: *Numerical K_T, as a function of the ratio of structure height (h_c) to water depth (d). Compared with Allen and Webb 2011 shell bag breakwater K_T (Allen and Webb, 2011).*

The Keulegan-Carpenter number, a dimensionless number characterized by the ratio of inertial forces to drag forces, was used to understand the drag mechanism responsible for wave dissipation. The KC number is generally used to study wave forces on submerged, bluff marine structures and is defined by:

11

$$KC = \frac{u_m T}{L}$$

where u_m is the maximum horizontal particle velocity, analogous to the wave orbital velocity previously calculated, T, is the wave period, and L is the size or length scale of the structure (Sorensen, 1978). Maximum horizontal particle velocities were measured in the highest and lowest water depth numerical simulations at a depth of 0.3 m, around the middle of the oyster cage at the same distances used for across flume elevation measurements. The L value was varied from 0.15 to 1.20 to show how the KC number would change based on the wave interaction with one oyster (0.15 m) to the length of the entire cage (1.2 m).

.

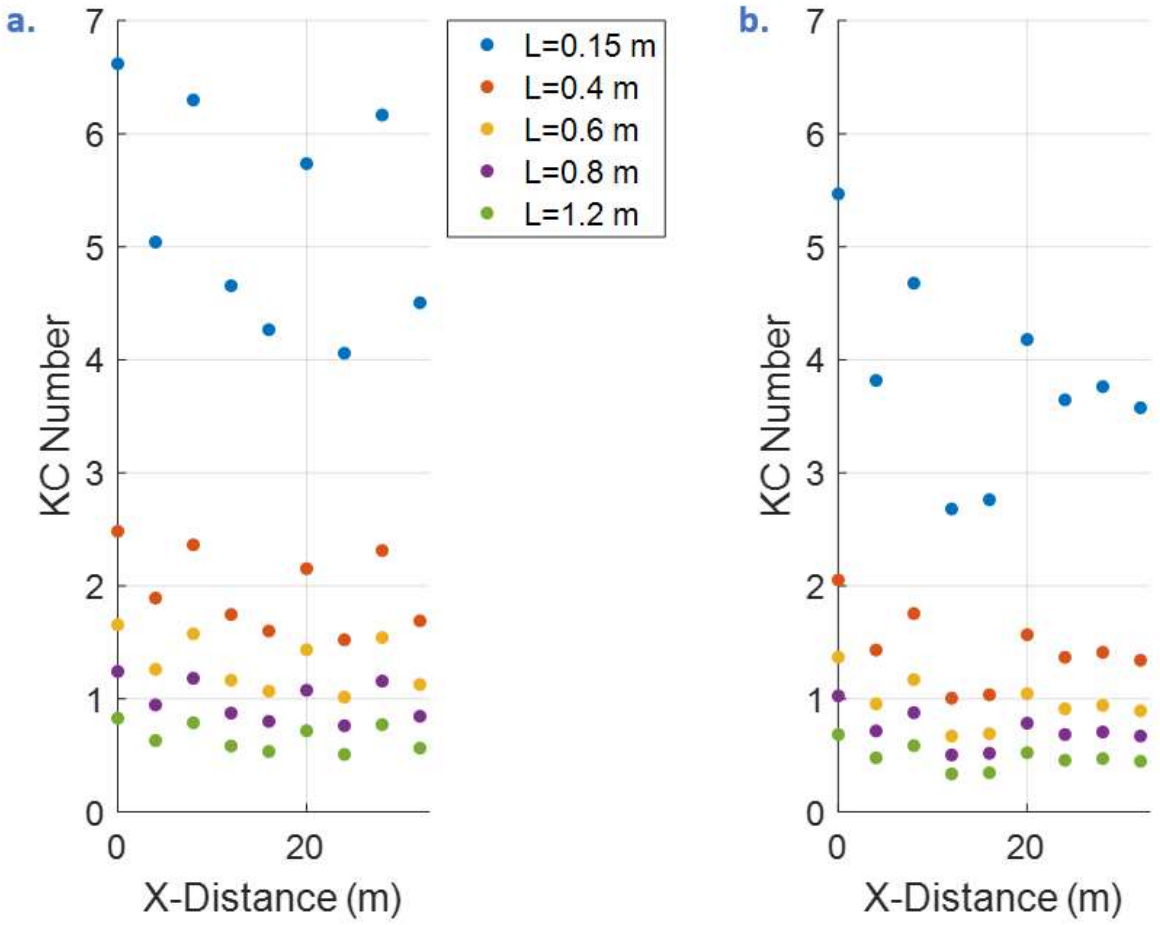

Figure 17: *Keulegan-Carpenter Numbers for a. 2.33 m depth and b. 5.34 m depth cases.*

Inertial forces dominate at KC < 5 and drag forces dominate at KC >25 with mixed domination in between (Sorensen, 1978). KC numbers along the longline were mostly below 5 for both high (Figure 17a) and low (Figure 17b) water depth cases, indicating inertia dominated wave interaction with the structures. Thus, wave attenuation was caused by an added mass force rather than drag on the water, as the porosity of the cage allowed for more wave interaction with the inner oyster bags. KC numbers were seen to increase generally along the flume, as wave decay progressed, indicating that wave attenuation became more and more inertial based than drag

along the farm. For the same wave environment used in this study, KC numbers for Allen and Webb (2011) could be as high as 15 due to a smaller characteristic length of the width of their bag (0.076 m). This suggests that oyster cages act more prominently as a bluff body, promoting wave attenuation through added mass, while oyster shell bag breakwaters are influenced less so by inertial forces and drag becomes more important. To predict wave decay over oyster long lines of different sizes over varying water depths and wave conditions, the usage of an empirical formula would be very useful.

The numerical model results were compared to an empirical equation for a submerged rubble mound breakwater. The line of 10 cages is investigated as a line of 10 individual breakwaters, with each having their own transmission coefficient, K_{T_n}. The formula developed by Seabrook and Hall (1998), referred to herein as SH98, was selected for its implementation of breakwater armored rock diameter as sink in wave attenuation due to internal flow losses and surface friction and for its applicability in previous shellfish based coastal protection media (Sigel, 2021). The SH98 solution was originally tested for 11 irregular wave cases, thought to be typical of design conditions, with K_T values evaluated spectrally as $\frac{H_{m0_T}}{H_{m0_I}}$,. The design equation for transmission at a single submerged rubble mound breakwater is as follows (Hall & Seabrook, 1998):

12

$$K_{T_n} = 1 - \left[e^{-.65\left(\frac{d_s}{H_i}\right) - 1.09\left(\frac{H_i}{B}\right)} + 0.047\left(\frac{Bd_s}{LD_{50}}\right) - 0.067\left(\frac{d_s H_i}{BD_{50}}\right) \right]$$

where d_s is the depth to the top of the breakwater, H_i is the incident significant wave height, B is the width of the breakwater, L is the local wavelength, and D_{50} is the median stone diameter. All dimensions are representative of one oyster cage. Transmission coefficient, K_T is defined as the ratio of H_{s_t} to H_{s_i}. Progressive wave decay can be measured by the following equation, where the K_{T_n} changes as a function of the incident wave moving across the line of oyster cages.

13

$$H_{n+1} = K_{T_n} * H_{i_n}$$

H_{n+1} is the wave height over the next oyster cage, K_{t_n} is the SH98 design wave transmission coefficient for the singular oyster cage, and H_{i_n} is the propagating wave height over the oyster cage.

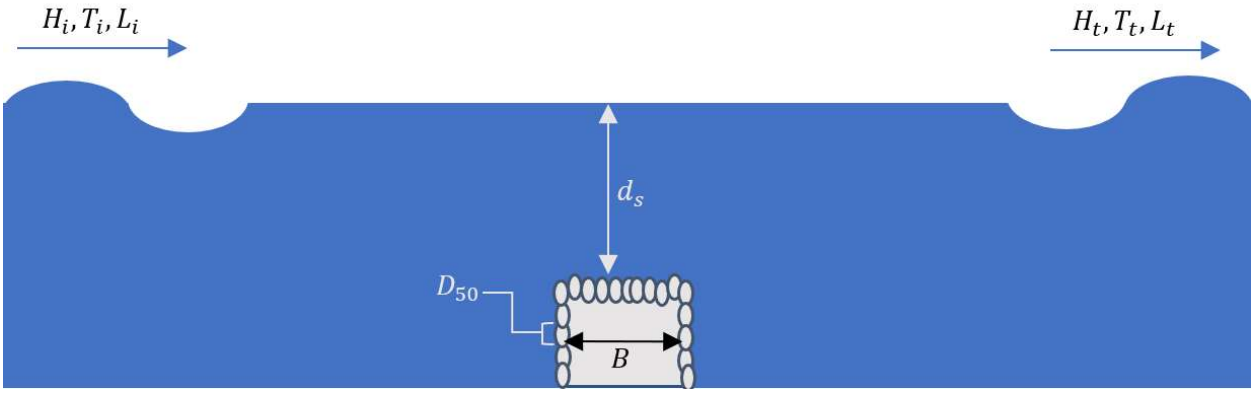

Figure 18: *Nomenclature for design equation of submerged rubble mound breakwater from SH98, where* $H_i. T_i, L_i$ *are the incident wave height, period, and length respectively, and* $H_t. T_t, L_t$ *are the transmitted wave height, period, and length respectively.*

Average wave height decay along the long line of cages was compared with SH98, which accounts for gain of attenuation (decrease in K_T) through flow through the breakwater using the $\frac{Bd_s}{LD_{50}}$ term and accounts for loss in attenuation (increase in K_T) through frictional dissipation on the structure using the $\frac{d_s H_i}{BD_{50}}$ term. Tuning of the median stone diameter to match the results of the numerical simulations led to a D_{50} of 0.20 meters to be forced in the design equation. This D_{50} is larger than what was used in testing of SH98, where the value is between 0.017 m and 0.037 m, but in other studies has been implemented as high as 0.30 m (Bredes et al., 2022). This allowed for a good fit to the numerical results along the long line for lower water depth cases. The D_{50} term is not indicative of any dimension associated with the geometry of the interior bags or individual oyster shells but is parametrized to match the "porosity" seen visually in the numerical flume, modeled by the small block cages. The D_{50} chosen is close to the length of the oysters, which can be thought of has a proxy porosity for the breakwater interior. The porosity of the oyster cages can be estimated by:

14

$$\phi = \frac{V_v}{V_T}$$

Where V_v is the volume of the voids (volume of cage not occupied by oyster bags) and V_T is the volume of the cage. Porosity for a cage was found to be 0.413, consistent with porosity for armored stone breakwaters, studied to be between 0.25 and 0.40, with higher porosity for larger armored stones (Latham et al., 2006). The porosity calculation in equation 14 is most likely an overestimation of the porosity due to the voids created by the oysters inside the bags themselves.

These results from the SH98 solution aligned favorably with SPH results for along farm decay when considering each oyster cage as an independent breakwater (Figure 19). Wave decay was seen to be closest to numerical results for the shallowest water depth studied, which can be attributed to the high depth dependency of the empirical breakwater formula. For increasingly deeper water depths, the SH98 solution tended to overestimate the attenuation when compared with the numerical solution (Figure 18). It is possible that the floating interior bags created a variable d_s, when bags settled to the bottom or floated to the top, that altered the depth dependent parts of equation 11. The tuning parameter, D_{50}, could also not be constant at all water depths and may need to be tuned in the future.

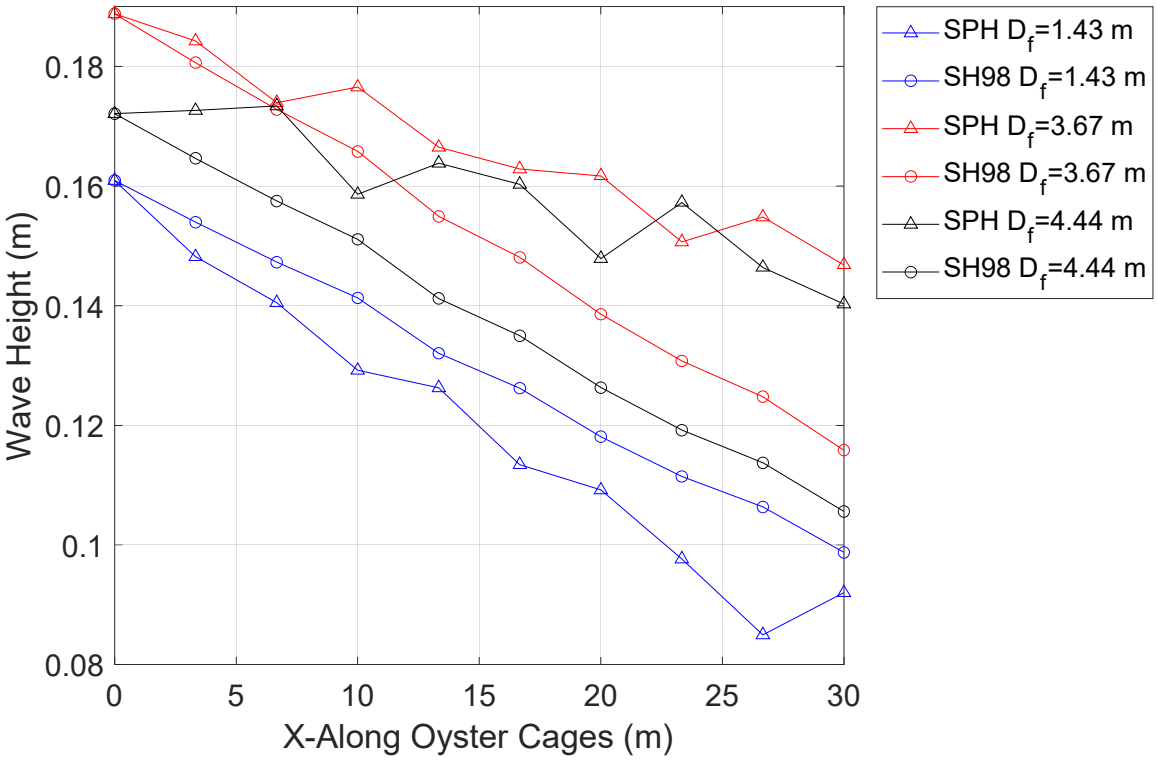

Figure 19: *Along farm decay from SPH numerical flume, compared with Seabrook and Hall (SH_P) 1998 solution for submerged breakwaters.*

Using the tuned SH98, a low water depth scenario was examined for extreme wave height decay to understand applicability in a shallower environment. A 1.0 m depth, 0.20 m incident wave height and 20 m wavelength (height and wavelengths consistent with other cases) scenario was tested and showed very high wave attenuation results. The wave height was dissipated from 20 to 3.2 cm for this case along the long line (Figure 19). The low water depth causes a much steeper exponential decay than seen in the deeper water depths from the test cases due to the exponential $e^{-.65\left(\frac{d_S}{H_i}\right)-1.09\left(\frac{H_i}{B}\right)}$, with the majority of the attenuation occurring over the first 15 m of the line of cages. Implementation of oyster long lines or grids in shallower water could have attenuation close to 100% during a low depth period (< 1.0 m). It's critical to note that depending on the starting stage of the tide, these low depth scenarios could leave the oysters emergent at lower stages of the tide, which could be harmful to oyster health and growth. Additionally, wave decay of this magnitude over a short distance could greatly increase radiation stress gradients over an oyster farm, resulting in changes to the mean water level that could influence local currents. These factors should be considered carefully in oyster cage coastal defense design.

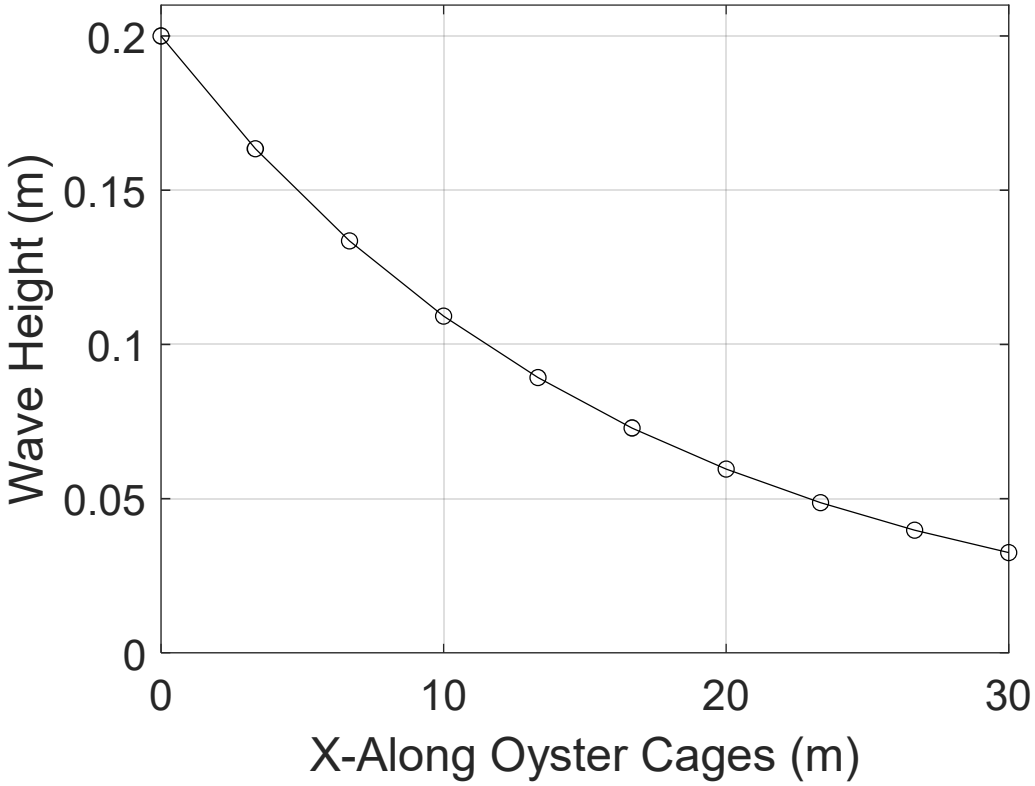

Figure 20: *Wave decay of 0.20 meter wave at 0.40* d_o *(1.0 m depth) using the tuned Seabrook and Hall solution.*

Given that significant wave decay is expected in shallower water depths, it is likely that these longitudinal changes in radiation stresses would influence the mean water levels, much like that observed over coral reefs (Buckley et al. 2016). Using the cross-shore momentum balance equation, changes to water level along the farm due to wave decay can be calculated. The following momentum balance can be used to investigate changes to water level in the presence of wave decay and tidal currents (Buckley et al., 2016; Raubenheimer et al., 2001):

15

$$\frac{\partial S_{xx}}{\partial x} + \tau_b + \rho g(\eta + h)\frac{\partial \eta}{\partial x} = 0$$

where τ_b is the bottom stress, defined by $\rho C_d \overline{|u_b| u_b}$ and u_b is the cross-shore velocity above the bottom, C_d is the bottom drag coefficient assumed to be 0.03, also used in Buckley et al, 2016, $\frac{\partial S_{xx}}{\partial x}$ is the cross-farm wave radiation stress gradient. S_{xx} is measured longitudinally by:

16

$$S_{xx} = \frac{3}{2}E$$

where E is the wave energy, $E = \frac{1}{16}\rho g H_s^2$, ρ is the water density, η is the water level and h is the water depth. Setup or set down can be calculated as the change in η along the area of interest, derived from the momentum balance as follows (Buckley et al., 2016; Raubenheimer et al., 2001):

17

$$\bar{\eta} = \int_{-h}^{\eta} \frac{-\tau_b - \frac{\partial S_{xx}}{\partial x}}{\rho g h} dx$$

For less dramatic wave decay, a lower wave radiation stress is observed, leading to relatively low setup along the long line (Figure 21). A very shallow depth empirical wave decay case with variable bottom current, u_b was examined. For wave decay over the long line in 1 m of water depth (not observed in the field), set up was seen to vary from 5.88 mm to 4.11 cm for bottom currents acting against the wave direction between 0.2 m/s and 0.6 m/s (Figure 20). For waves

propagating onshore, currents in opposition to wave propagation create the highest setup and would be expected during ebb tide when tidal currents are moving out of the bay. High wave decay combined with very strong tidal currents would cause the largest setup- potentially causing barotropic flow depending on the size of the farm and morphology of the basin.

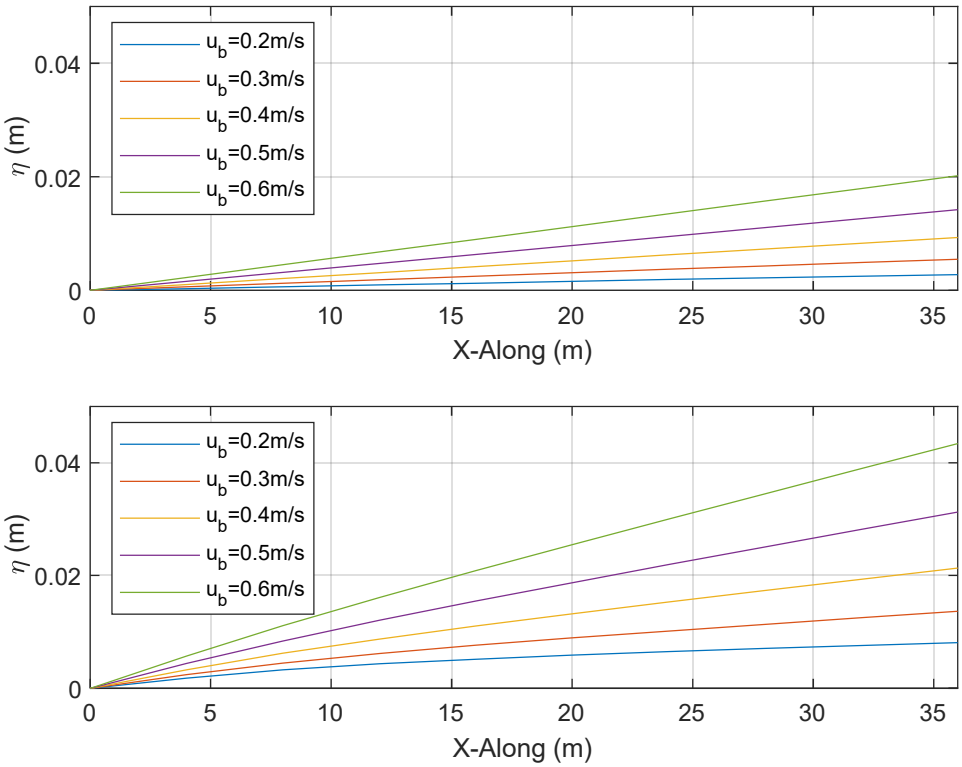

Figure 21: *Water level across long line of oyster cages for wave decay for 4 second waves for a. 2.3 m depth and b. 1.0 meter depth scenario.*

The potential influence on mean water levels is important to placement and design of oyster cages as coastal protection in semi-enclosed bays. Wave setup can drive currents due to the cross-shore barotropic pressure gradients interacting with a boundary, which may alter

circulation and transport and should be considered when placing this type of coastal protection in shallower water.

From an industry perspective, the implementation of an existing breakwater design equation can allow for layout design of oyster cages as a coastal protection system. The layout of a line of breakwaters is not a traditional approach to a breakwater system. Traditionally one line of a breakwater would be laid out perpendicular to a wave ray, spanning a distance to cover a certain onshore or nearshore area. The implementation of submerged breakwaters has a large limitation in Maine waters due to the large tidal range. Using the Seabrook and Hall equation, wave transmission coefficients for the entire long line ranged from 0.35 to 0.68 for d of 1.95 and 5.34 m respectively (Figure 15). Wave transmission decreased by 14% with a 3.1 m difference in depth. In Maine, where tidal ranges can be as high as 5.6 meters and storm tides can add an additional 1.5+ meters, the variability of wave attenuation performance poses a problem in submerged breakwater design. However, a wave transmission coefficient of 0.68 in an enclosed bay is significant. In laboratory studies of submerged rubble-mound breakwaters, Hassanpour, et al. (2023) found wave transmission coefficients ($K_T = \frac{H_t}{H_i}$) between 0.8 and 0.2 for submerged structures, indicating comparable results to a line of oyster cages. Naturally, the line of cages would encompass more area in a design site than a single breakwater, and would need to be arranged in successive lines or arrays in order to prevent refraction and diffraction around a single line. These cages could be placed in a location where they would always be submerged, to encourage oyster growth, but in a shallower area, to maximize the wave attenuation capabilities of the cages.

Additionally, seasonality could have large impacts on wave attenuation properties of oyster cages. In enclosed bays, where waves are highly dependent on wind, cages need to be placed in an orientation where they are attenuating waves for a protected location of interest. The offshore propagating waves seen in this study are not common to all bays and seasonal time frames, and wave direction and seasonal wind direction must be considered in this longitudinal type of design in enclosed environments.

The direct measurement of radiation stresses and tidal currents were not measured by the instrumentation on site and can be considered as limitations to this study. Drifting in the buoys due to scope on the line during low tide also could have created several scenarios where the buoys were not lined up over the longline domain, and wave characteristic changes could have been independent of the oyster cages. Additionally, the macrotidal waters created a highly fluctuating depth throughout the data collection period, and water depths on site were much larger than water depth used in previous literature. Some inaccuracies could have propagated in the numerical model. Computational cost limited by the time of simulations only allowed for an interparticle distance of 2 cm and a 2-dimensional domain. A lowered dpi could have impacted wave propagation over the oyster cages, and additionally could have given the opportunity to more finely design the oyster cages in the numerical model. The 2-dimensional model also ignored any directional impacts to wave attenuation and width-based wave impacts from the cages. However, these limitations also simplified the experimental domain, such that results can be more compared to more controlled results from laboratory experiments or empirical formulas.

CONCLUSION

Short ($2.5 < T < 4s$), coastal wind waves in a sheltered bay environment can be attenuated by submerged oyster aquaculture cages up to 40% through inertial forces. For the waves studied in the field, shorter waves and less steep waves were attenuated more. Wave decay was found to be mostly linear along the long line of oyster cages, similar to results of other aquaculture based longitudinal wave decay (Zhu et al., 2021). Wave decay was seen to increase in shallow water environments and a smaller dimensionless freeboard, the ratio of significant wave height to water depth, H_s/d, consistent with findings from previous shellfish-based wave attenuation studies (Allen & Webb, 2011; Chauvin, 2018; Sigel, 2021). This study reinforces previous investigations that shellfish-based structures can reduce wave energy, while adding new insight on the inertial based wave attenuation mechanism and wave-induced set-up over the structures. These finding furthers the research thrust of nature-based coastal protection, by seeking coastal defense from existing placed food-based aquaculture systems. Oyster farming, while important to the state of Maine's economy, is a large international industry, and implementation of aquaculture based coastal protection can be an option around the world. Due to their depth dependence, longitudinal decay from oyster cages would be most effective in meso to microtidal regimes, and would be less effective in macrotidal waters, however punctilious depth-based design as well as communication with farmers on oyster growth submergence needs will allow for this design in the future. Findings in this study are promising toward furthering the implementation of aquaculture based coastal protection, however, further research into broader wave regimes, as well as other depths and farm scales will be crucial to understand before implementation in engineering design.

CHAPTER 3

The overarching goal of this research was to investigate the wave attenuation capabilities of bottom-lying oyster aquaculture gear commonly utilized by Maine oyster farmers. This was accomplished through a field campaign in Casco Bay, measuring waves over a part of an overwintered oyster farm, and through a numerical model of the field site. At shallow water depths, wind waves can be attenuated effectively using bottom lying oyster cages. With proper consideration of the macrotidal, fluctuating water depths in Maine, oyster cages could prevent some long-term erosion of beaches and bluffs. Cages may struggle to provide adequate protection during storm surge events, when water levels rise too high for bottom cage wave attenuation effectiveness. Waves impact bluff erosion indirectly by removing slumped debris below the bluff, which sets up future erosion, a process which occurs over a quite large timescale- decades to centuries (Whiteman et al., 2016). A reduction in wave energy around bluffs in Maine could have large impacts on long term bluff erosion. Sea levels will continue to rise, storms will continue to grow stronger, due to mostly irreversible impacts to this planet's changing climate. Any coastal protection with feasibly positive results that also benefits the economy as well as natural habitats should be investigated with due diligence. With further research into the effectiveness at lower water depths, as well as attenuation over larger and denser farms, oyster farmers and coastal planners would have information that could help them plan oyster farms with coastal erosion in mind or use oyster cages directly has a form of coastal defense.

FUTURE WORK

Future work related to this project should focus on better preparation of both physical investigations and a SPH numerical model. Full scale laboratory testing of oyster cages in differing wave environments could provide much greater insight into wave attenuation and be more properly validated with a numerical model. The use of the SOFAR Spotter Wave Buoys in a shallow, sheltered environment caused many issues in data processing of wave observations that limited the breadth of waves that could be examined on the site. A future test on such a small domain should employ fixed wave gauges that can properly measure smaller waves. The use of the SOFAR buoys allowed for a baseline measurement of bulk parameters, that, when examined spectrally gave us an understanding of bulk wave parameters at the site. Proper wave gauges could allow for more accuracy and fixity in place of wave measurements. While we are grateful to Maine Ocean Farms for allowing this investigation to take place on their farm, a shallower and more exposed environment for oyster cage deployment could lead to richer results in the future. This limitation stems from the coastline of Maine, where much of the "working waterfront" lies in more sheltered than exposed areas. A long-term study of shoreline retreat in an area protected by oyster cages would give more primary results of oyster aquaculture as a coastal erosion prevention strategy as well.

DualSPHysics is a new software to researchers at the University of Maine, and due to computational costs and time constraints, the SPH numerical model accompanying this field study had some limitations. Future work should involve the utilization of other forcings in DualSPHysics, including inlet and outlet conditions for real-life wave spectra and currents. With

proper technology, higher resolution simulations could be run that could capture the movement of the oysters in the cages and provide greater insight into flow through the cage with high resolution post-processing.

APPLICATIONS

This study introduces and furthers the idea that Maine aquaculture can be coupled with a shoreline protection strategy. Taking oyster growth gear, something that has been designed and deployed for the sole purpose of food production in the ocean, and finding another purpose for it that does not harm its original purpose is exactly what this state needs to protect and promote its "working waterfront". This study, as well as previous and future studies at the University of Maine in aquaculture engineering can inform farmers and government bodies to begin strategizing the placement of systems so that their coastal engineering performance can be tapped into. This is the idea of a new living breakwater, where instead of cultivating natural ecosystems around a wave attenuation structure, the living organisms can be harvested for food production and economic gain. With the findings of this work, future research projects can be developed to study nuances in wave attenuation over this media so that, in the future, oyster cages can be an option for coastal protection for homeowners and municipalities.

REFERENCES

Allen, R. J., & Webb, B. M. (2011). Determination of wave transmission coefficients for oyster shell bag breakwaters. *Coastal Engineering Practice - Proceedings of the 2011 Conference on Coastal Engineering Practice*. https://doi.org/10.1061/41190(422)57

Altomare, C., Domínguez, J. M., Crespo, A. J. C., González-Cao, J., Suzuki, T., Gómez-Gesteira, M., & Troch, P. (2017). Long-crested wave generation and absorption for SPH-based DualSPHysics model. *Coastal Engineering*, *127*. https://doi.org/10.1016/j.coastaleng.2017.06.004

Bredes, A. L., Miller, J. K., Kerr, L., & Brown, D. R. (2022). Observations of Wave Height Amplification Behind an Oyster Castle Breakwater System in a High-Energy Environment: Gandys Beach, NJ . In *Frontiers in Built Environment* (Vol. 8). https://www.frontiersin.org/articles/10.3389/fbuil.2022.884795

Buckley, M. L., Lowe, R. J., Hansen, J. E., & Van Dongeren, A. R. (2016). Wave Setup over a Fringing Reef with Large Bottom Roughness. *Journal of Physical Oceanography*, *46*(8), 2317–2333. https://doi.org/https://doi.org/10.1175/JPO-D-15-0148.1

Chauvin, J. M. (2018). *Wave Attenuation by Constructed Oyster Reef Breakwaters*. https://digitalcommons.lsu.edu/gradschool_theses

Chen, H., Liu, X., & Zou, Q.-P. (2019). Wave-driven flow induced by suspended and submerged canopies. *Advances in Water Resources*, *123*, 160–172. https://doi.org/https://doi.org/10.1016/j.advwatres.2018.11.009

Emlein, M. C. (2021). Rising to the Challenge: Managed Retreat and the Taking Clause in Maine's Climate Change Era. *Me. L.Rev.*

Garzon, J. L., Maza, M., Ferreira, C. M., Lara, J. L., & Losada, I. J. (2019). Wave Attenuation by *Spartina* Saltmarshes in the Chesapeake Bay Under Storm Surge Conditions. *Journal of Geophysical Research: Oceans*, *124*(7). https://doi.org/10.1029/2018JC014865

Giles, M. L., Sorensen, R. M., & (U.S.), C. E. R. C. (1978). *Prototype scale mooring load and transmission tests for a floating tire breakwater* . U.S. Army, Corps of Engineers, Coastal Engineering Research Center. https://www.biodiversitylibrary.org/item/102192

Gormley, M., & MacLeod, S. (2021). Towards a Solid Particle Hydrodynamic (SPH)-Based Solids Transport Model Applied to Ultra-Low Water Usage Sanitation in Developing Countries. In *Water* (Vol. 13, Issue 4). https://doi.org/10.3390/w13040441

Hall, K. R., & Seabrook, S. R. (1998). Design Equation for Transmission at Submerged Rubblemound Breakwaters. *Journal of Coastal Research*, 102–106. http://www.jstor.org.wv-o-ursus-proxy02.ursus.maine.edu/stable/25736126

Ji, C.-Y., Chen, X., Cui, J., Yuan, Z.-M., & Incecik, A. (2015). Experimental study of a new type of floating breakwater. *Ocean Engineering*, *105*, 295–303. https://doi.org/https://doi.org/10.1016/j.oceaneng.2015.06.046

Kamphuis, J. W. (2010). Introduction to Coastal Engineering and Management. In *Advanced Series on Ocean Engineering: Vol. Volume 30*. WORLD SCIENTIFIC. https://doi.org/doi:10.1142/7021

Latham, J.-P., Meulen, J. A., & Dupray, S. (2006). The specification of armourstone gradings and EN 13383 (2002). *Quarterly Journal of Engineering Geology and Hydrogeology - Q J ENG GEOL HYDROGEOL*, *39*, 51–64. https://doi.org/10.1144/1470-9236/05-025

Main Sea Grant. (2013). Overwintering of Eastern Oysters: Guidance for Small-Scale Growers. *University of Maine Cooperative Extension*.

Maine Coast Fishermen. (2022). *Working Waterfront*. https://www.mainecoastfishermen.org/working-waterfront

Maine Revenue Service. (2020). *Working Waterfront Tax Law FAQ*. maine.gov/revenue/faq/working-waterfront

Manis, J. E., Garvis, S. K., Jachec, S. M., & Walters, L. J. (2015). Wave attenuation experiments over living shorelines over time: a wave tank study to assess recreational boating pressures. *Journal of Business and Psychology*, *30*(1). https://doi.org/10.1007/s11852-014-0349-5

Morris, R. L., Bilkovic, D. M., Boswell, M. K., Bushek, D., Cebrian, J., Goff, J., Kibler, K. M., La Peyre, M. K., McClenachan, G., Moody, J., Sacks, P., Shinn, J. P., Sparks, E. L., Temple, N. A., Walters, L. J., Webb, B. M., & Swearer, S. E. (2019). The application of oyster reefs in shoreline protection: Are we over-engineering for an ecosystem engineer? In *Journal of Applied Ecology* (Vol. 56, Issue 7). https://doi.org/10.1111/1365-2664.13390

Morris, R. L., Graham, T. D. J., Kelvin, J., Ghisalberti, M., & Swearer, S. E. (2019). Kelp beds as coastal protection: wave attenuation of Ecklonia radiata in a shallow coastal bay. *Annals of Botany*. https://doi.org/10.1093/aob/mcz127

O'Donnell, J. E. D. (2017). Living Shorelines: A Review of Literature Relevant to New England Coasts. In *Journal of Coastal Research* (Vol. 33, Issue 2). https://doi.org/10.2112/JCOASTRES-D-15-00184.1

Piazza, B. P., Banks, P. D., & La Peyre, M. K. (2005). The potential for created oyster shell reefs as a sustainable shoreline protection strategy in Louisiana. *Restoration Ecology*, *13*(3). https://doi.org/10.1111/j.1526-100X.2005.00062.x

Plew, D. R., Stevens, C. L., Spigel, R. H., & Hartstein, N. D. (2005). Hydrodynamic implications of large offshore mussel farms. *IEEE Journal of Oceanic Engineering*, *30*(1), 95–108. https://doi.org/10.1109/JOE.2004.841387

Raubenheimer, B., Guza, R. T., & Elgar, S. (2001). Field observations of wave-driven setdown and setup. *Journal of Geophysical Research: Oceans*, *106*(C3), 4629–4638. https://doi.org/https://doi.org/10.1029/2000JC000572

Schmitt, C. (2017). All About Maine Oysters. *Maine Sea Grant Publications*, *157*.

Scyphers, S. B., Powers, S. P., Heck, K. L., & Byron, D. (2011). Oyster reefs as natural breakwaters mitigate shoreline loss and facilitate fisheries. *PLoS ONE*, *6*(8). https://doi.org/10.1371/journal.pone.0022396

Sigel, L. (2021). *Effect of an artificial oyster reef on wave attenuation*. TU Delft.

Sinnett, G. (2012). *Circulation and transport in Casco Bay, Maine*. University of Maine.

Slovinsky, Peter, Schmitt, C. (2011). *Building a Resilient Coast: Maine Property Owner's Guide to Managing Flooding, Erosion and Other Coastal Hazards*.

Sorensen, R. M. (1978). *Basic Coastal Engineering*.

Spaulding, M. (2011). *REVIEW OF CIRCULATION STUDIES AND MODELING IN CASCO BAY*.

Whiteman, N., Kelley, J. T., Belknap, D. F., & Dickson, S. M. (2016). *Coastal Bluff Erosion, Landslides and Associated Salt Marsh Environments in Northern Casco Bay, Maine* (Vol. 326).

Zhu, L., Huguenard, K., Zou, Q. P., Fredriksson, D. W., & Xie, D. (2020). Aquaculture farms as nature-based coastal protection: Random wave attenuation by suspended and submerged canopies. *Coastal Engineering*, *160*. https://doi.org/10.1016/j.coastaleng.2020.103737

Zhu, L., Lei, J., Huguenard, K., & Fredriksson, D. W. (2021). Wave attenuation by suspended canopies with cultivated kelp (Saccharina latissima). *Coastal Engineering*, *168*. https://doi.org/10.1016/j.coastaleng.2021.103947

APPENDICES:

APPENDIX A: Comparison of Numerical and Field Spectrums Studied for 34 validation Cases

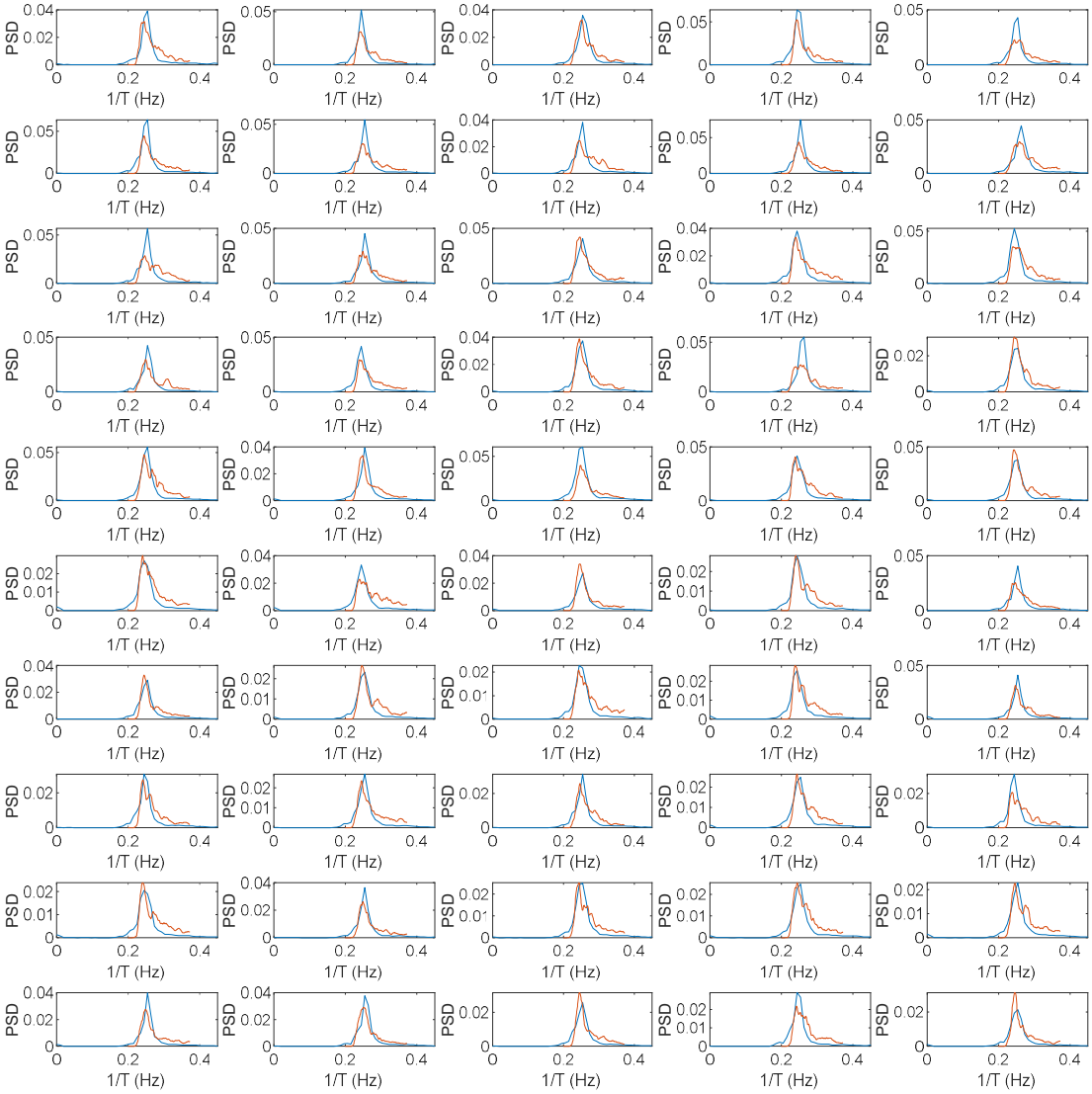

Appendix A: Spectra generated by numerical piston in DualSPHysics in blue, compared with field spectra in orange.

Appendix B: Example XML Structure of DualSPHysics Simulations

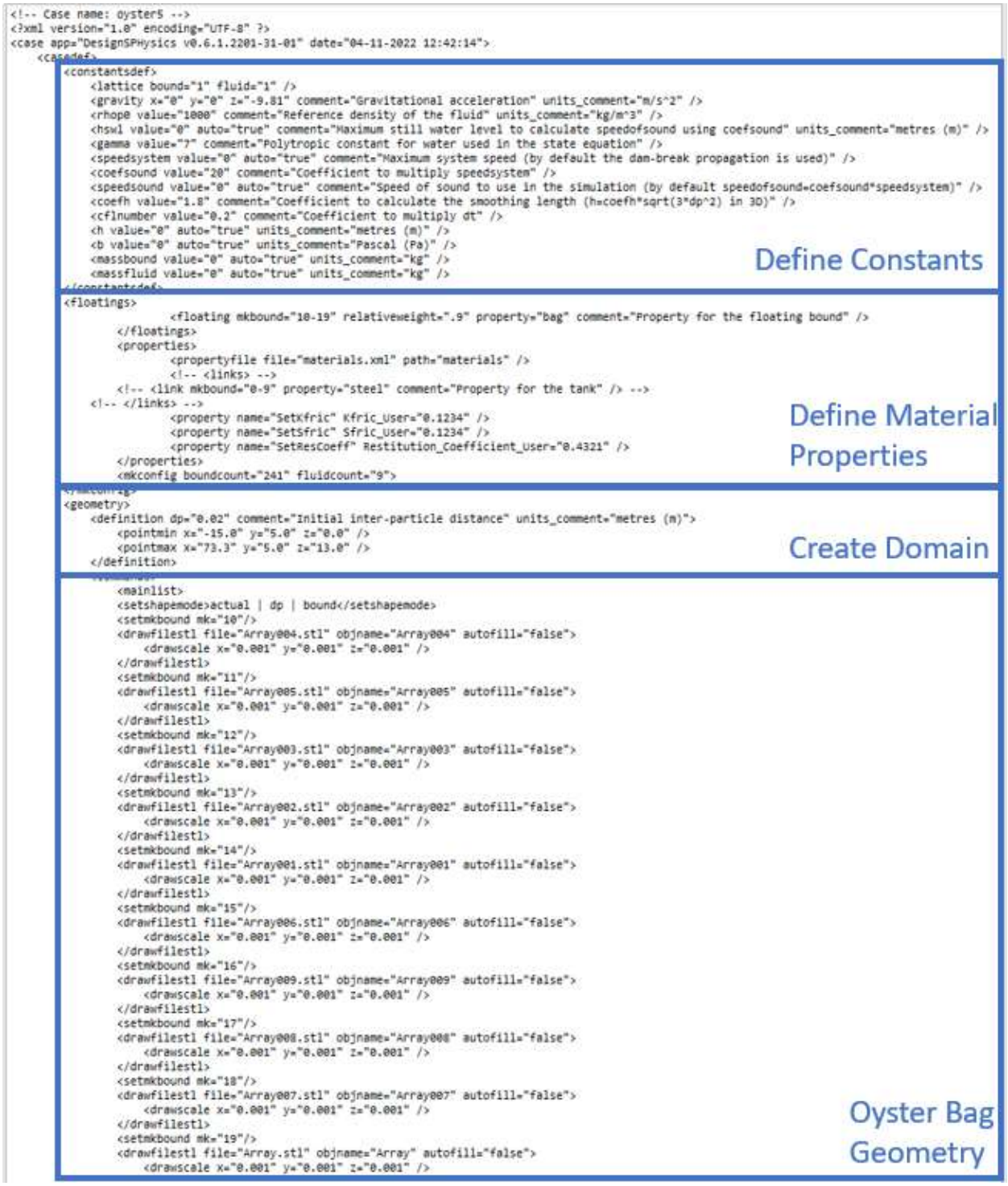

```
</drawfilestl>
 <setmkbound mk="0"/>
<drawfilestl file="LinkGroup.stl" objname="Cage" autofill="false">
    <drawscale x="0.001" y="0.001" z="0.001" />
</drawfilestl>
<setmkbound mk="1"/>
<drawfilestl file="LinkGroup001.stl" objname="Cage001" autofill="false">
    <drawscale x="0.001" y="0.001" z="0.001" />
</drawfilestl>
<setmkbound mk="2"/>
<drawfilestl file="LinkGroup002.stl" objname="Cage002" autofill="false">
    <drawscale x="0.001" y="0.001" z="0.001" />
</drawfilestl>
<setmkbound mk="3"/>
<drawfilestl file="LinkGroup003.stl" objname="Cage003" autofill="false">
    <drawscale x="0.001" y="0.001" z="0.001" />
</drawfilestl>
<setmkbound mk="4"/>
<drawfilestl file="LinkGroup004.stl" objname="Cage004" autofill="false">
    <drawscale x="0.001" y="0.001" z="0.001" />
</drawfilestl>
<setmkbound mk="5"/>
<drawfilestl file="LinkGroup005.stl" objname="Cage005" autofill="false">
    <drawscale x="0.001" y="0.001" z="0.001" />
</drawfilestl>
<setmkbound mk="6"/>
<drawfilestl file="LinkGroup006.stl" objname="Cage006" autofill="false">
    <drawscale x="0.001" y="0.001" z="0.001" />
</drawfilestl>
<setmkbound mk="7"/>
<drawfilestl file="LinkGroup007.stl" objname="Cage007" autofill="false">
    <drawscale x="0.001" y="0.001" z="0.001" />
</drawfilestl>
<setmkbound mk="8"/>
<drawfilestl file="LinkGroup008.stl" objname="Cage008" autofill="false">
    <drawscale x="0.001" y="0.001" z="0.001" />
</drawfilestl>
<setmkbound mk="20"/>
<drawfilestl file="LinkGroup009.stl" objname="Cage009" autofill="false">
    <drawscale x="0.001" y="0.001" z="0.001" />
</drawfilestl>
<setmkbound mk="9"/>
<setdrawmode mode="full"/>
<drawbox objname="piston">
    <boxfill>solid</boxfill>
    <point x="-10.0" y="2.5" z="0.0" />
    <size x="0.20" y="5.0" z="12.0" />
                    <layers vdp="-0.5" />
</drawbox>

<setdrawmode mode="full"/>
<drawbox objname="floc">
    <boxfill>solid</boxfill>
    <point x="-17.0" y="2.5" z="-.15" />
    <size x="56.3" y="5.0" z="0.20" />
                    <layers vdp="-0.5" />
</drawbox>
<move x="38.3" y="2.5" z="0.0" />
<rotate ang="11.999999999999808" x="-0.0" y="1.0" z="-0.0" />
<setmkbound mk="22"/>
<setdrawmode mode="full"/>
<drawbox objname="Beach">
    <boxfill>solid</boxfill>
    <point x="0" y="0" z="-.15" />
    <size x="35.0" y="5.0" z="0.20" />
                    <layers vdp="-0.5" />
</drawbox>
<matrixreset />
<move x="-13.0" y="2.5" z="0.0" />
<setmkfluid mk="0"/>
<fillbox x="15.0" y="2.5" z="1.5" objname="FillBox">
    <modefill>void</modefill>
    <point x="0" y="0" z="0" />
    <size x="78.3" y="5.0" z="1.545" />
</fillbox>
<matrixreset />
<shapeout file="" />
</mainlist>
```

Oyster Cage Geometry

Piston Geometry

Flume Geometry

Water Geometry

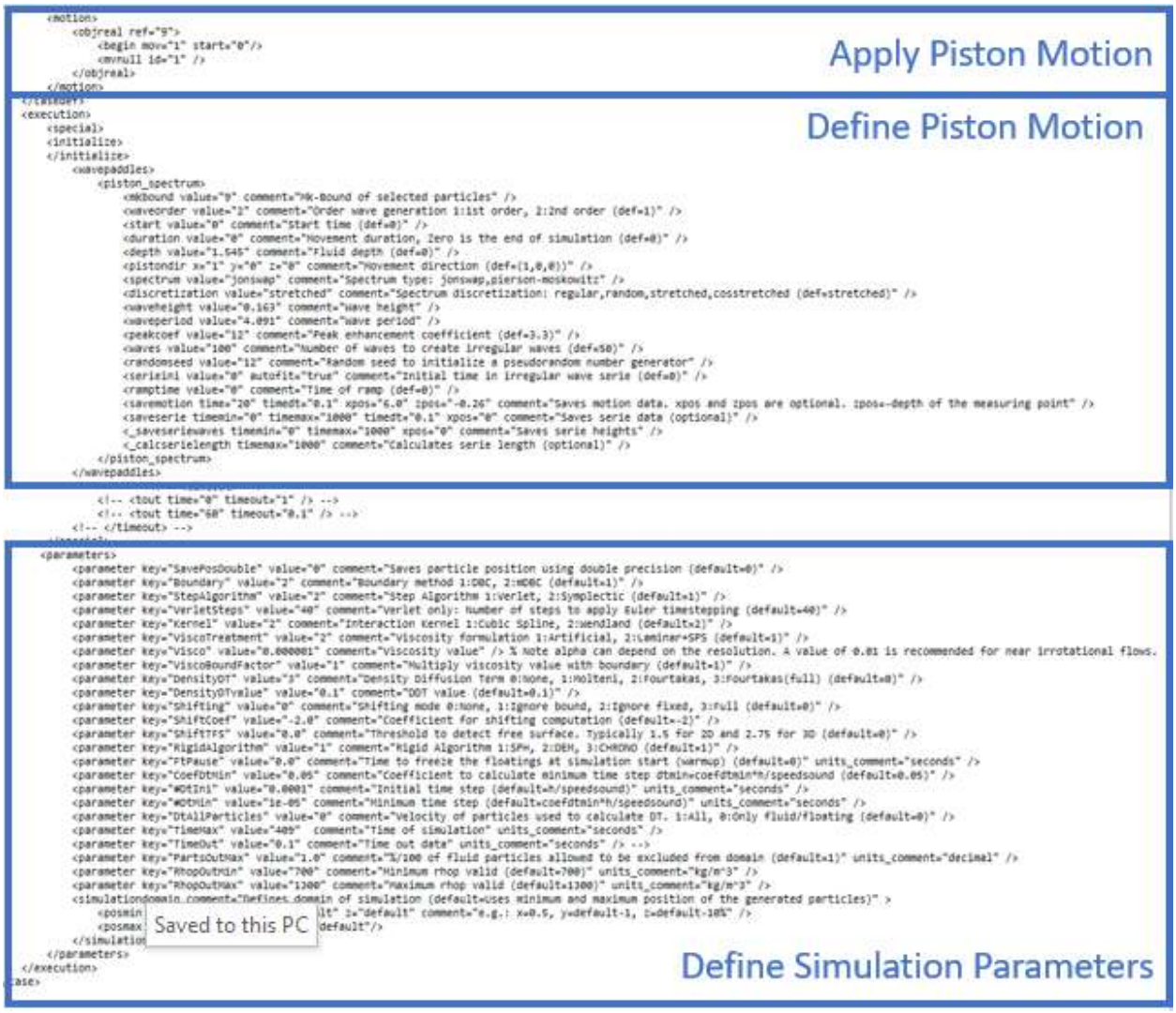

Appendix B: XML code that defines the parameters of the DualSPHysics numerical simulation. Variables of water depth, peak period, and significant wave height were changed for each run.

Appendix C: SOFAR Spotter Specifications

Spotter Technical Specifications

SOFAR

Specs

External dimensions [w X h]	42 cm x 31 cm (16.4 in x 12.2 in)
Weight	7.45 kg (16 lbs, 7 oz)
Connectivity	Iridium SBD (satellite)
Primary power source	Solar powered, 5x 2 Watt, 6 Volt solar panels
Battery	Lithium-ion, capacity 11,200 mAh, 3.7v (rechargeable)

Motion Sensing

Motion data format	Easting, northing, elevation, latitude, longitude
Wave frequency range	0.03-1 Hz (30s to 1s)
Wave direction resolution	0 - 360 degrees (full circle)
Sampling rate	2.5 Hz (Nyquist at 1.25Hz)
Wave displacement accuracy	Approximately +/- 2cm accuracy depends on field of view, weather conditions, and GPS system status
Calibration	Not needed, ever

Additional Onboard Sensors

Sea surface temperature (SST)	-5°C to 50°C range, ±0.1°C absolute accuracy, ±0.02°C resolution
Barometer	Range: 700...1100mbar, Accuracy: +/-0.5 mbar at 25°C

Data Storage

On-board (SD card)	Records time series of 3D displacement data, ships with 16GB (256GB max capacity). FAT16 or FAT32 Format required
Cloud storage (online dashboard)	Online account includes: Real-time and historical data outputs, Spotter configurations, alerts, maps and 2-way communication

Data Outputs

* Can derive from SD card data.

	Standard mode	Spectrum mode	On device
Significant wave height	x	x	x*
Peak period	x	x	x*
Mean period	x	x	x*
Peak direction	x	x	x*
Mean direction	x	x	x*
Peak directional spread	x	x	x*
Mean directional spread	x	x	x*
Variance density spectrum		x	x
Directional moments (a1, b1, a2, b2)		x	x
3D displacement time series @ 2.5 Hz (x,y,z)			x
Sea surface temperature		*Not available with Smart Mooring units.*	
Wind speed	x	x	
Wind direction	x	x	x*
Drift speed			x*
Drift direction			x*
Geographical coordinates (lat, lon)	x	x	x*

Misc. specs

System monitoring	Battery power status
Advised mooring depth	Any depth
Visibility LED	1 flash every 2.5 sec, at least 1 mile visibility under normal conditions.
Firmware upgrade	Standard micro-USB (cable included)
Usability	Magnetic on/off switch, run/idle mode, user LED's and integrated grab handles.

www.sofarocean.com

Appendix C: Specifications provided by SOFAR Spotter Buoys used in wave data collection.

Appendix D: HOBO Water Level Logger Specifications

Pressure (Absolute) and Water Level Measurements U20L-01	
Operation Range	0 to 207 kPa (0 to 30 psia); approximately 0 to 9 m (0 to 30 ft) of water depth at sea level, or 0 to 12 m (0 to 40 ft) of water at 3,000 m (10,000 ft) of altitude
Factory Calibrated Range	69 to 207 kPa, 0° to 40°C (10 to 30 psia, 32° to 104°F)
Burst Pressure	310 kPa or 18 m depth (45 psia or 60 ft depth)
Water Level Accuracy*	Typical error: ±0.1% FS, 1.0 cm (0.03 ft) water Maximum error: ±0.2% FS, 2.0 cm (0.06 ft) water
Raw Pressure Accuracy**	±0.3% FS, 0.62 kPa (0.09 psi) maximum error
Resolution	<0.02 kPa water (0.007 ft water)
Pressure Response Time (90%)***	<1 second at a stable temperature; measurement accuracy also depends on temperature response time

Appendix D: Specifications provided by HOBO Water Level Logger used in water level measurement at the field site.

BIOGRAPHY OF THE AUTHOR

Liam Hanley was born in Danbury, Connecticut on March 15, 1999. He grew up in New Fairfield, Connecticut and graduated from New Fairfield High School in 2017. He attended the University of Connecticut and graduated with a bachelor's degree in civil engineering in 2021. During his undergraduate studies he held many internship positions in structural and coastal engineering at firms in Connecticut and Rhode Island. Upon completion of his bachelors, he decided to pursue a master's degree in coastal engineering to further his knowledge in a growing industry. He started his graduate studies at the University of Maine in the fall of 2021. Upon completion of his masters, Liam will begin his career in coastal engineering design and consulting with GZA GeoEnvironmental Engineers in Providence, Rhode Island. He is a candidate for the Master of Science degree in Civil Engineering from the University of Maine in August 2023.